Determination of Far-Field Antenna Patterns from Near-Field Measurements

RICHARD C. JOHNSON, H. ALLEN ECKER, AND J. SEARCY HOLLIS

Invited Paper

***Abstract*—In many cases, it is impractical or impossible to make antenna pattern measurements on a conventional far-field range; the distance to the radiating far field may be too long, it may be impractical to move the antenna from its operating environment to an antenna range, or the desired amount of pattern data may require too much time on a far-field range. For these and other reasons, it is often desirable or necessary to determine far-field antenna patterns from measurements made in the radiating near-field region; three basic techniques for accomplishing this have proven to be successful. In the first technique, the aperture phase and amplitude distributions are sampled by a scanning field probe, and then the measured distributions are transformed to the far field. In the second technique, a plane wave that is approximately uniform in amplitude is created by a feed and large reflector in the immediate vicinity of the test antenna. And in the third technique, the test antenna is focused within the radiating near-field region, patterns are measured at the reduced range, and then the antenna is refocused to infinity. Each of these techniques is discussed, and the various advantages and limitations of each technique are presented.**

INTRODUCTION

IN MANY CASES, it is impractical or impossible to measure antenna patterns[1] on a conventional far-field range; the distance to the radiating far field may be too long, it may be impractical to move the antenna from its operating environment to an antenna range, or the desired amount of pattern data may require too much time on a far-field range. For these and other reasons, it often is desirable or necessary to determine far-field antenna patterns from measurements made in the radiating near-field region; three basic techniques for accomplishing this have proven to be successful. After presenting introductory material, each of these techniques will be discussed, and the various advantages and limitations of each technique will be presented.

Field Regions

An antenna is a device for transforming a guided wave into a wave radiated in space, or vice versa, and the distribution of field strength about an antenna is, in general, a function of both the distance from the antenna and the angular coordinates. Since it is our objective to determine antenna radiation patterns, it is instructive first to consider the nature of the field regions surrounding an antenna.

In the region close to an antenna, the field will include a reactive component as well as a radiating component. The strength of this reactive component, however, decays rapidly with distance from the antenna so that it soon becomes insignificant compared to the strength of the radiating component. That region in space in which the reactive component of the field predominates is called the *reactive near-field region*, and beyond this region, the radiating field predominates.

That region in which the radiating field predominates is further subdivided into the *radiating near-field region* and the *radiating far-field region*. In the radiating near-field region, the angular distribution of radiated energy is dependent on the distance from the antenna; whereas, in the radiating far-field region, the angular distribution of radiated energy is essentially independent of distance from the antenna.

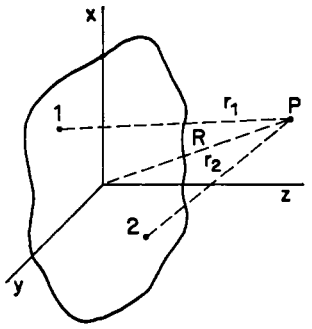

Fig. 1. Schematic representation of a planar antenna aperture in the x–y plane, an observation point P, and distances to the observation point from the origin and two elements of the antenna.

In the radiating near-field region, the relative phases and the relative amplitudes of contributions from various elements of the antenna are functions of the distance from the antenna. To visualize this situation refer to the schematic representation of Fig. 1. For simplicity, assume that the antenna is planar and is located in the x–y plane; the distances to the observation point P from two arbitrary elements of the antenna are represented by r_1 and r_2. Notice that as the observation point is moved farther from the origin, in a fixed angular direction, the relative distance to the arbitrary elements (r_2 minus r_1) changes; this causes the relative phases and amplitudes of contributions from elements 1 and 2 to change with distance from the antenna. By extending this argument to include all contributing elements of the antenna, one sees that the measured radiation pattern of the antenna will depend upon the radius to the observation point.

When the distance to the observation point gets very large, straight lines from any two contributing elements to the observation point (r_1 and r_2, for example, in Fig. 1) are essentially parallel and the ratio r_1/r_2 is essentially unity. Thus at large distances, the relative phases and amplitudes of con-

This invited paper is one of a series planned on topics of general interest—The Editor.

Manuscript received February 6, 1973; revised June 20, 1973.

R. C. Johnson and H. A. Ecker are with the Engineering Experiment Station, Georgia Institute of Technology, Atlanta, Ga. 30324.

J. S. Hollis is with Scientific-Atlanta, Inc., Atlanta, Ga. 30332.

[1] An antenna pattern is a graphical representation of the radiation properties of an antenna as a function of direction. When discussing an antenna, one usually describes its properties as a transmitting antenna. The *reciprocity theorem*, however, states that the directional pattern of a receiving antenna is identical with its pattern as a transmitting antenna provided it contains no unilateral or nonlinear devices [1].

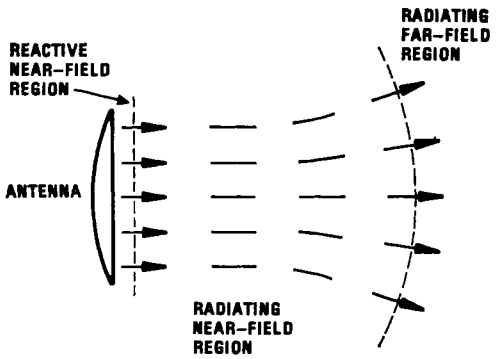

Fig. 2. Pictorial representation of the three regions surrounding an antenna.

tributions from the various elements change very slowly with distance, and the angular distribution of radiated energy measured at such large distances is essentially independent of the distances to the observation point. This condition is indicative of the radiating far-field region.

Thus the space surrounding an antenna is composed of three regions: the reactive near-field region, the radiating near-field region, and the radiating far-field region [2]. These three regions are shown pictorially in Fig. 2. The boundaries between the regions are not well defined, but for any antenna the reactive near-field region extends only a short distance [3]. The commonly accepted distance to the boundary between the reactive and radiating near-field regions is $\lambda/2\pi$. For electrically large antennas of the aperture type, such as that depicted in Fig. 2, the commonly used criterion to define the distance to the boundary between the radiating near-field and far-field regions is [4]

$$R = \frac{2D^2}{\lambda} \tag{1}$$

where D is the largest dimension of the aperture and λ is the wavelength.

Although the aforementioned criterion to define distance to the far-field region is generally accepted and is used quite widely, one must always remember that it is an arbitrary choice and that it is inadequate for some special situations. For example, if one must accurately measure patterns of antennas having very low sidelobes or if one must make accurate gain measurements of pyramidal horns which have large phase deviations across their apertures, the measurement distance may have to be much longer than $2D^2/\lambda$.

Arguments have been advanced for decreasing or for increasing the accepted distance to the boundary between the near-field and far-field regions; however, $2D^2/\lambda$ seems to be the most popular choice. The situation is analogous to trying to decide the ideal height for a stepladder. Most of us might agree that 2 m is an ideal height, but there will be special jobs which require a higher ladder and other jobs in which a shorter ladder is acceptable.

It has been customary in the past to refer to field regions as *Fresnel* or *Fraunhofer*, after the approximations described. As pointed out by Hansen [3], this practice should be discouraged. It is better to define field regions as reactive near field, radiating near field, and radiating far field as discussed earlier and illustrated in Fig. 2. Then, the terms Fresnel and Fraunhofer can be used more correctly to refer to analytical approximations.

Pattern Measurements

Most aperture antennas are designed to transmit a beam over long distances; therefore, it is desirable to know certain features of the radiation pattern in the radiating far field. Since the conventional procedure is to operate the test antenna in a receiving mode,[2] it is desirable to illuminate the test antenna with a uniform plane wave. The creation of such a wave is a difficult task, however, so one usually resorts to approximation methods.

The conventional procedure for approximating a uniform plane wave is to locate a transmitting antenna at such a distance that the incident wave can be considered to be plane. In an ideal situation in which the transmitter is located $2D^2/\lambda$ away from the test antenna, the spherical wavefront emitted from the transmitter will produce a maximum phase deviation of $\pi/8$ at the edge of the antenna aperture. As mentioned previously, however, there are special situations in which such a phase deviation is too large, and in these cases, distances greater than $2D^2/\lambda$ must be used.

Besides the phase deviation due to the spherical wavefront emitted by the transmitter, other serious problems can arise due to unwanted reflections from the ground and surrounding objects on an antenna range. Normally, one desires to measure free-space patterns which imply a single source of energy reaching the test antenna; however, unwanted reflections from the surroundings can cause measurement errors.

As the separation between the transmitting antenna and test antenna increases, it becomes more difficult to keep unwanted reflections from the ground and surrounding objects below acceptable levels. Also, for very large antennas and for very short wavelengths, the distance to the radiating far field may be so long that it is impractical or impossible to make the measurements on a conventional range. In addition, many antennas cannot be moved from their operating environment to an antenna range, and with some antennas, such as phased arrays, the desired amount of pattern data may require enormous measurement time on a conventional antenna range.

For those and other reasons it often is desirable to determine far-field antenna patterns from measurements made in the radiating near-field region; three basic techniques for accomplishing this have proven to be successful. In the first technique, the aperture phase and amplitude distributions are sampled by a scanning field probe, and then the measured distributions are transformed to the far field. In the second technique, a plane wave that is approximately uniform in amplitude is created by a feed and large reflector in the immediate vicinity of the test antenna. And in the third technique, the test antenna is focused within the radiating near-field region, patterns are recorded at the reduced range, and then the antenna is refocused to infinity.

The above techniques will be presented in more detail in the following three sections, and then all three techniques will be discussed in the concluding remarks.

Transformation of Near-Field Measurement Data to Obtain Far-Field Patterns

Background

When antennas are very large or when the final stages of assembly occur at the installation site, the direct measurement of accurate far-field patterns is extremely difficult and often

[2] An antenna usually is tested in a receiving mode because it is convenient to connect the pattern recording equipment located near the antenna under test.

impossible. Some investigators have resorted to the use of aircraft [5], earth satellites [6], or celestial bodies [7] as a measurement site or source to achieve the required far-field distance for antenna measurements. As an alternative to the direct measurement of far-field patterns, the mathematical transformation of measured near-field data can produce accurate far-field patterns.

Two fundamentally different principles have been applied in attempts to determine far-field antenna patterns from measurements of the near field of an antenna. Initial efforts were inspired by the principle that the complete electromagnetic field configurations surrounding an antenna can be computed if either the current or charge distribution over the antenna structure is known exactly [8]. Thus work centered on accurate measurements of the tangential magnetic $\boldsymbol{H}$ field in very close proximity to the antenna structure [9]–[11]. For aperture antennas, the Huygens–Fresnel Principle [4, ch. 4] was utilized to form an equivalent source from the aperture field distributions. The Huygens–Fresnel Principle states that each point on a given wavefront can be regarded as a secondary source that gives rise to a spherical wavelet. The field at any point exterior to the wavefront can be derived from a superposition of these elementary wavelets. The Equivalence Theorem given by Schelkunoff [12] provides a rigorous mathematical treatment of the Huygens–Fresnel Principle applied to electromagnetic waves.

The second method for determining far-field patterns from near-field measurements is based on expressing the total electromagnetic field in terms of a modal expansion. The amplitudes and phases of these modes can be derived from measurements of the electromagnetic field over an appropriate surface in the near field, for example, a plane surface for a plane-wave expansion or a cylindrical surface for a cylindrical-wave expansion. However, the exact distance of the surface from the antenna is usually not critical. Knowledge of the amplitude and phase of each component in the modal expansion permits a complete description of the radiated field and therefore the far-field radiation pattern.

The following sections describe the two basic methods for determining far-field patterns by transformation of near-field measurement data: 1) direct determination of source distribution from near-field measurements and 2) modal expansion and determination of mode characteristics from near-field measurements. Typical results are presented and advantages and disadvantages of the two methods are identified.

Far-Field Determination from Source Distributions Derived from Near-Field Measurements

Basic Concepts: It can be shown that the complete electric $\boldsymbol{E}$ and magnetic $\boldsymbol{H}$ fields within a given volume can be expressed in terms of the current densities of the sources within the volume and the values of the field itself over the boundaries of the volume. This result is obtained by applying a vector Green's Theorem to the pair of vector Holmholtz equations representing the electric and magnetic fields in the volume. If the volume of interest is defined to contain no sources and to be bounded by a closed surface S and the sphere at infinity, the $\boldsymbol{E}$ and $\boldsymbol{H}$ fields at a point P within the volume are shown by Silver [4, ch. 9] to be

$$\boldsymbol{E}_p = \frac{1}{4\pi}\int_s [-j\omega\mu(\hat{n}\times\boldsymbol{H})\psi + (\hat{n}\times\boldsymbol{E})\times\nabla\psi + (\hat{n}\cdot\boldsymbol{E})\nabla\psi]da \quad (2)$$

$$\boldsymbol{H}_p = \frac{1}{4\pi}\int_s [j\omega\epsilon(\hat{n}\times\boldsymbol{E})\psi + (\hat{n}\times\boldsymbol{H})\times\nabla\psi + (\hat{n}\cdot\boldsymbol{H})\nabla\psi]da \quad (3)$$

where $\hat{n}$ is the unit vector normal to the surface. The function ψ is the scalar portion of the Green's function and is given by

$$\psi = \frac{e^{-jkr}}{r} \quad (4)$$

where k is the free space wavenumber and r is the distance from a point on the surface to a field point. The function ψ satisfies the radiation condition with the result that the values of the above surface integrals over the sphere at infinity are zero. Also, all sources are assumed to be enclosed by the surface S.

When it is desirable to determine the current or charge distribution on the surface of the antenna rather than the field distribution in an aperture, the closed surface S is assumed to be perfectly conducting and the boundary conditions

$$\hat{n}\times\boldsymbol{E} = 0 \qquad \hat{n}\times\boldsymbol{H} = \boldsymbol{K}$$
$$\hat{n}\cdot\boldsymbol{E} = \frac{\rho_s}{\epsilon} \qquad \hat{n}\cdot\boldsymbol{H} = 0 \quad (5)$$

are applied, where $\boldsymbol{K}$ is the surface current density and ρ_s is the surface charge density. If, in addition, the equation of continuity relating current density and charge density is utilized, the equations for the $\boldsymbol{E}$ and $\boldsymbol{H}$ fields can be expressed in terms of either current density or charge density alone. In terms of survace current density on the perfectly conducting surface S, the electric and magnetic fields at a point P in the volume of interest then can be expressed as

$$\boldsymbol{E}_p = -\frac{j}{4\pi\omega\epsilon}\int_s [(\boldsymbol{K}\cdot\nabla)\nabla + k^2\boldsymbol{K}]\frac{e^{-jkr}}{r}da \quad (6)$$

$$\boldsymbol{H}_p = \frac{1}{4\pi}\int_s (\boldsymbol{K}\times\nabla)\frac{e^{-jkr}}{r}da. \quad (7)$$

Thus in its fundamental formulation, the method of determining field patterns from source distributions involves the application of (2) (3) for aperture distributions or (6) and (7) for current distributions. In the first case, near-field measurements are made to determine the $\boldsymbol{E}$ and $\boldsymbol{H}$ field distributions over a surface surrounding the antenna, whereas, in the second case, measurements of tangential $\boldsymbol{H}$ or normal $\boldsymbol{E}$ fields very close to the physical structure of the antenna are made to evaluate surface current densities or surface charge densities. Equations (6) and (7) can be expressed in terms of charge densities rather than current densities by application of the equation of continuity.

Except for very simple geometries, (2), (3), (6), and (7) are extremely difficult or impossible to apply without approximations. These approximations usually relate to the nature of the fields or currents on the surface over which the integration is performed. The approximations that are necessary to permit evaluation of the surface integrals usually fall into one of the following areas:

1) assuming negligible contribution of the fields or currents over some portion of the surface;
2) assuming all radiation follows outward normals to the surface;

3) assuming the electric and magnetic fields are linearly related as in a plane wave;
4) assuming small-angle approximations and thus limiting the angular region for locating the field point.

Approximations of this type should be distinguished from the normal far-field approximations that simplify computation but produce valid results at distances sufficiently far from the source to satisfy far-field conditions discussed in the Introduction.

Near-Field Probing: Investigators of this source distribution method for determination of far-field patterns have concentrated on near-field measurement techniques intended to permit an accurate description of the source amplitude and phase distributions. Richmond and Tice [13] have investigated the desired characteristics for a probe to be suitable for microwave near-field measurements. Their criteria for a suitable probe are the following:

1) Any distortion of the fields by the probe and the associated equipment must not seriously affect the accuracy of the measurement.
2) The aperture of the probe must be small enough to measure essentially the field at a point.
3) The probe must have the desired polarization to a high degree of accuracy.
4) The probe must deliver a signal voltage large enough to permit accurate measurements.

Borts and Woonton [14], [15] have studied the effect of the directivity of the probe on measurements of aperture fields. A variety of probes including shielded loops, tapered waveguides, electric dipoles, and biconical antennas were investigated. Probes of the size of half-wave dipoles or smaller were determined to be necessary for accurate measurements of the field. Probes with more directivity than half-wave dipoles were found to produce large measurement errors. This work was done mainly with field distributions in circular apertures to permit an empirical correction factor developed by Andrews [16] to be used in the calculation of the fields. Andrews interprets his empirical relationship as the result of interference between the primary wave in the aperture and secondary waves from the edge of the aperture. A brief description of aperture edge effects and associated approximations will be given later.

Plonsey [17] has shown that under certain conditions, an electric probe can be used for the measurement of surface distributions. In his method, an electric monopole is used to measure the rate of change of electric field to determine the magnetic field and thus the surface current. The accuracy of the method is limited by the approximation of the partial derivative of the tangential electric field with respect to the distance from the conducting surface by the expression

$$\frac{\partial E_{\tan}}{\partial \rho} = \frac{E_{\tan}(\Delta\rho)}{\Delta\rho} \tag{8}$$

where $\Delta\rho$ is the distance of the probe from the conducting surface. A comparison of measured and calculated results indicates that accurate measurements of reflector surface currents with an electric probe can be achieved if probe-reflector distances no greater than $\lambda/20$ are used. An evaluation of errors introduced by interaction between probe and reflector indicated that interaction errors were acceptable for this spacing. The chief source of error appeared to be in the accuracy with which the position of the probe relative to the reflector could be measured.

The most common technique for measuring the magnetic field and thus the source current distribution is the small-loop antenna. Whiteside and King [18] investigated the properties of small circular and square-loop antennas for probes. Results are compared for theoretical calculations and measurements with singularly loaded and doubly loaded loops. It was determined that the diameter of singularly loaded loops must be maintained less than 0.01λ to prevent large measurement errors, whereas, doubly loaded loops could achieve comparable accuracy with diameters as large as 0.15λ.

The open-ended waveguide or small horn is a very useful near-field probe in the microwave region. In contrast to the dipole probe fed by a coaxial cable, these probes require no balun to obtain satisfactory results. Richmond and Tice [13] have investigated the effect of size of waveguide probes on the measurement of phase and amplitude distributions in the near field. Dielectrically filled waveguides covered with absorbing materials were used to obtain small aperture probes. When operating probes at 9.375 GHz ($\lambda = 3.2$ cm), they found that a dielectrically filled open-ended waveguide with dimensions of 0.46 cm by 1.07 cm gave essentially the same results as a probe with aperture size 0.36 cm by 0.71 cm; whereas, probes with larger apertures gave significantly different results. Good agreement between calculated and measured far-field patterns from a horn were obtained when the smallest aperture probe was used to measure the aperture distribution of the horn for the computation of the far-field pattern. Their results indicate that probe aperture areas less than $\lambda^2/16$ are required for accurate near-field measurements.

Justice and Rumsey [19] have developed a technique for measuring near-field distributions based on detecting the reflected wave from a thin, straight, conducting scatterer placed in the unknown field. Although straightforward in theory, careful attention to instrumentation is required to implement this technique properly. A very carefully matched hybrid is required to achieve the necessary isolation to separate the reflected signal from the transmitted signal. Thus the fine balance required on this hybrid junction makes a very stable frequency source a necessity. Also, care must be taken in choosing the length-to-diameter ratio of the scatterer to discriminate between mutually perpendicular fields. Justice and Rumsey indicate that this technique operated successfully at 3 GHz and at 10 GHz. Richmond and Tice [13] show that when using the scattering technique at 9.375 GHz, a scatterer of length no greater than 0.76 cm ($\sim\lambda/4$) was required to achieve the same accuracies that can be obtained with small open-ended waveguide probes.

The scattering technique for measurement of near fields has been extended by Cullen, Parr, and Richmond [20], [21] by producing modulation on the scattered fields to make separation of the scattered field from the incident field easier. Hu [22] used two diodes in a small loop of wire, such that the scattered field from the magnetic moment of the loop was modulated but the scattered field due to the electric moment was not modulated. Harrington [23] has shown that the backscattered fields can be greatly enhanced if the scattering object is loaded to produce a resonance. When short dipoles and small loops are loaded to produce resonance, an improvement of the order of 30 dB can be obtained over the scattered field from nonresonant scatterers.

Pattern Computation and Associated Approximations

The computation of far-field patterns from source distributions derived from near-field measurements has its most

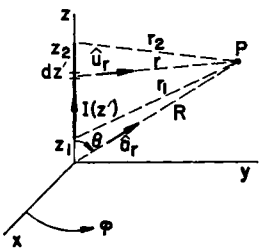

Fig. 3. Geometry for electric-current line source and an external field point P.

TABLE I

COMPARISON DATA OF MEASURED AND CALCULATED VALUES FOR LINE-SOURCE ANTENNA

(From Gamara, [27])

	Measured	Calculated
Half-power beamwidth	3.6°	3.5°
Tenth-power beamwidth	7.4°	7.0°
First-order zero right-side location	5.8°	6.15°
First-order zero left-side location	6.5°	5.9°
Second-order zero right-side location	10.5°	9.5°
Second-order zero left-side location	9.5°	9.5°
First-order sidelobe magnitude right-side location	18.8 dB	21.7 dB
First-order sidelobe magnitude left-side location	25.7 dB	24.2 dB

useful applications in situations in which either the geometry of the surface of the source can be made very simple as in a line source or the angular region of interest in the far field can be restricted to the main beam and close-in sidelobes. For the case of a line source, the surface integrals in (6) and (7) reduce to line integrals and the ϕ component of the magnetic field in the far-field region can be expressed simply as

$$H_\phi = \frac{jk \sin\theta e^{-jkR}}{4\pi R} \int_{z_1}^{z_2} I(z') e^{jkz' \cos\theta} dz' \tag{9}$$

when the geometry is as shown in Fig. 3 and the following far-field approximations can be applied:

1) the distance r, except in the phase term, can be replaced by R, the distance from the field point to the origin;
2) the value $1/r$ can be neglected in comparison with jk;
3) the directions of $\hat{a}_r$ and $\hat{a}_r$ can be considered parallel.

The θ component of the electric field can be derived from the magnetic field from the expression

$$E_\theta = \frac{k}{\omega\epsilon} H_\phi. \tag{10}$$

The application of (9) and (10) for determining far-field patterns from line sources is covered in many references [4, ch. 3], [24]. Also, Taylor [25], Ecker [26], and others have used the line source computation method to investigate far-field pattern synthesis. Gamara [27] has compared computed and measured far-field patterns from line sources and has analyzed sources of error. He concluded that good agreement can be achieved with relatively unsophisticated measurement equipment. A comparison of beamwidths, sidelobe levels, and null positions for measured and calculated patterns is shown in Table I for Gamara's line source.

Useful far-field patterns in the main-lobe region can be computed from relatively poor near-field data even for millimeter-wave antennas. A measured far-field pattern and the far-field pattern computed from crude measurements of the source distribution are shown in Fig. 4 for a 4.3-mm wave antenna, a folded geodesic Luneberg lens with a line source length of approximately 58.4 cm. [28]. Good agreement between calculated and measured patterns was achieved to below the −20-dB level. Also, the shoulders observed on the measured pattern between the −20-dB and −30-dB levels were predicted.

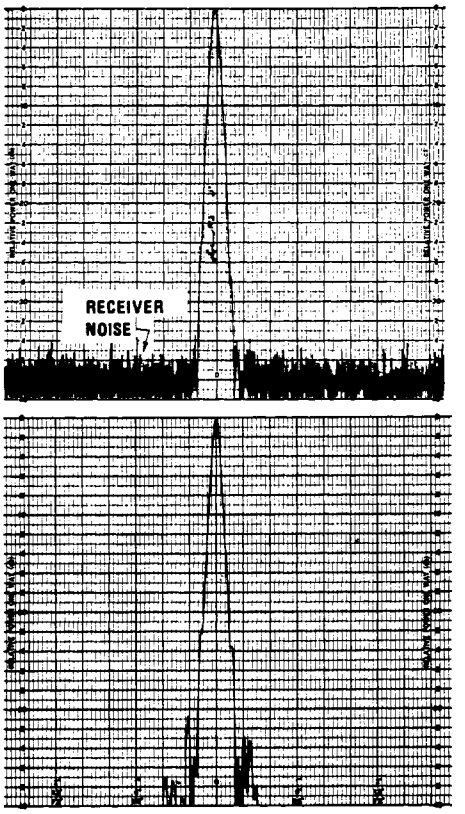

Fig. 4. Measured and computed far-field (H-plane) antenna patterns for a folded geodesic Luneberg lens antenna operating at 4.3 mm.

If planar apertures such as those that might be encountered in paraboloidal reflectors, horns, or slots are of interest, the source distribution is assumed to exist over a planar aperture in an opaque planar surface extending to infinity in both dimensions (see Fig. 5). For this geometry, (7) can be expressed as

$$E_p = -\frac{1}{4\pi}\int_A \left(\psi \frac{\partial E}{\partial n} - E\frac{\partial \psi}{\partial n}\right) da + \frac{1}{4\pi}\oint_c \psi(E \times \hat{\tau}) dl - \frac{1}{4\pi j\omega\epsilon}\oint_c \nabla\psi(\hat{\tau}\cdot H) dl \tag{11}$$

where $\hat{\tau}$ is the unit vector along the line integral contour. The magnetic field at P can be given in a similar form. We note that the initial term in (11) represents a surface integral over the aperture distribution whereas the second and third terms involve line contour integrals to account for the discontinuity at the edge of the aperture in the electric and magnetic fields, respectively. Silver [4, ch. 5] argues that for linear polarization and for small angles from the normal to the aperture the two contour integrals approximately cancel. Woonton [14]

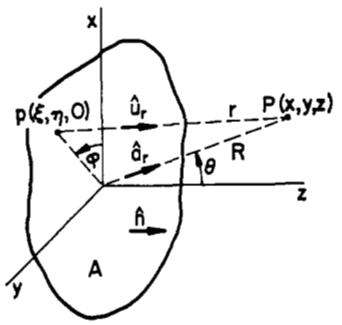

Fig. 5. Schematic representation of a planar aperture A in the x–y plane, an arbitrary point p in the aperture, and a field point P in the right hemisphere.

shows that Andrews' [16] empirical modification to the surface integral for circular apertures is an attempt to account for the effects of the two contour integrals.

For the assumptions of linear polarization and small angles, the equation for the electric field at a point can be reduced to the scalar integral

$$\mathcal{E}_p = -\frac{1}{4\pi}\int_A \left(\psi\frac{\partial \mathcal{E}}{\partial n} - \mathcal{E}\frac{\partial \psi}{\partial n}\right) da \tag{12}$$

in which the value of the integral is the particular linear component of the electric field at the point. This equation can be recognized as the Kirchhoff diffraction formula that is used in physical optics [29]. For the planar aperture shown in Fig. 5, Silver has reduced the scalar equation to apply for the previously given far-field criteria and to a restricted set of geometrical and field conditions. This scalar formulation of the far field from a planar aperture is given by the integral

$$\mathcal{E}(x, y, z) = \frac{j}{\lambda R} e^{-jkR}\int_A F(\xi, \eta) e^{jk \sin\theta(\xi\cos\phi + \eta\sin\phi)} da \tag{13}$$

where the field over the aperture is given by

$$F(\xi, \eta) = A(\xi, \eta) e^{-j\psi_p(\xi,\eta)} \tag{14}$$

and $A(\xi, \eta)$ and $\psi_p(\xi, \eta)$ are the aperture amplitude and phase distributions, respectively.

The restrictions on the utilization of the scalar formulation in (13) have been summarized by Paris [30] as follows:

1) harmonic time variations,
2) linear, homogenous, isotropic, and source-free medium,
3) zero tangential field intensities over the surface area outside the aperture,
4) negligible contributions of the intensities around the boundary of A,
5) plane aperture A,
6) short wavelengths,
7) $r \gg \lambda/2\pi$,
8) $\hat{n}\cdot\hat{u}_r \approx \hat{n}\cdot\hat{a}_r = \cos\theta$,
9) $e^{-jkr}/r \approx (e^{-jkr}/R)e^{jk \sin\theta(\xi\cos\phi+\eta\sin\phi)}$,
10) incidence of a TEM wave along the normal to the aperture,
11) $1+\cos\theta \approx 2$.

Paris has shown that by using the vector formulation for the far field in the diffraction problem more accurate results can be achieved. For this formulation only restrictions 1), 2), 3), and 7) from the previous list apply. Using the same geometry shown in Fig. 3, Paris expresses the electric and magnetic fields in vector form as

$$\boldsymbol{E}(x, y, z) = \frac{-jk}{4\pi}\int_A \hat{u}_r \times\left[(\hat{n}\times\boldsymbol{E}) - \sqrt{\frac{\mu}{\epsilon}}\,\hat{u}_r\times(\hat{n}\times\boldsymbol{H})\right]\frac{e^{-jkr}}{r} da \tag{15}$$

$$\boldsymbol{H}(x, y, z) = \frac{-jk}{4\pi}\int_A \hat{u}_r \times\left[(\hat{n}\times\boldsymbol{H}) - \sqrt{\frac{\epsilon}{\mu}}\,\hat{u}_r\times(\hat{n}\times\boldsymbol{E})\right]\frac{e^{-jkr}}{r} da. \tag{16}$$

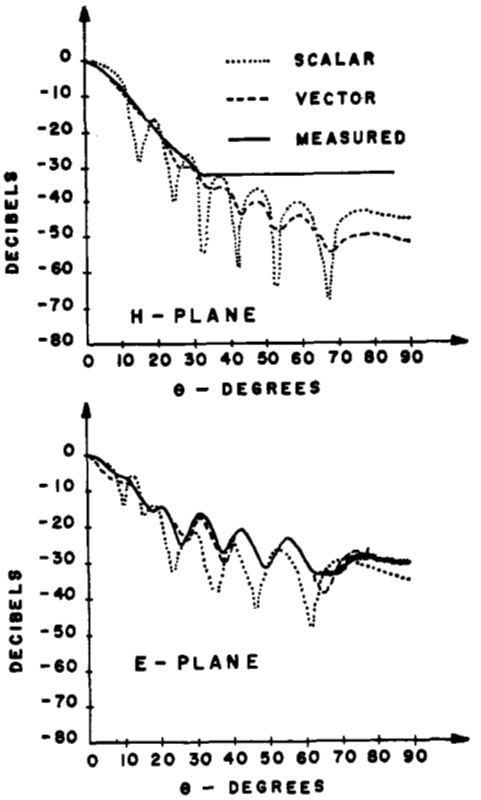

Fig. 6. Measured and computed E- and H-plane patterns of a standard gain horn operating at 16 GHz. Calculated patterns for scalar and vector formulations are shown. (From Paris, [39].)

Fig. 6 shows a comparison of measured patterns and computed patterns by the scalar and vector formulations for a pyramidal horn [30]. These data for $\boldsymbol{E}$ and $\boldsymbol{H}$-plane power patterns at 16 GHz indicate that much better agreement between measured and calculated results occurs when the vector formulation is used. Of course, considerably more complicated numerical techniques are necessary to implement the vector equations.

The development of systems for the simultaneous measurement of phase and amplitude of microwave fields has greatly facilitated near-field measurement techniques. Clayton, Hollis, and Teegarden [31] reported in 1961 the use of a microwave phase–amplitude measuring system to determine the near-field distribution of a 30.5-cm paraboloidal antenna operating at 13.5 GHz. They achieved a phase accuracy and stability of 5° and amplitude measurements within 0.5 dB

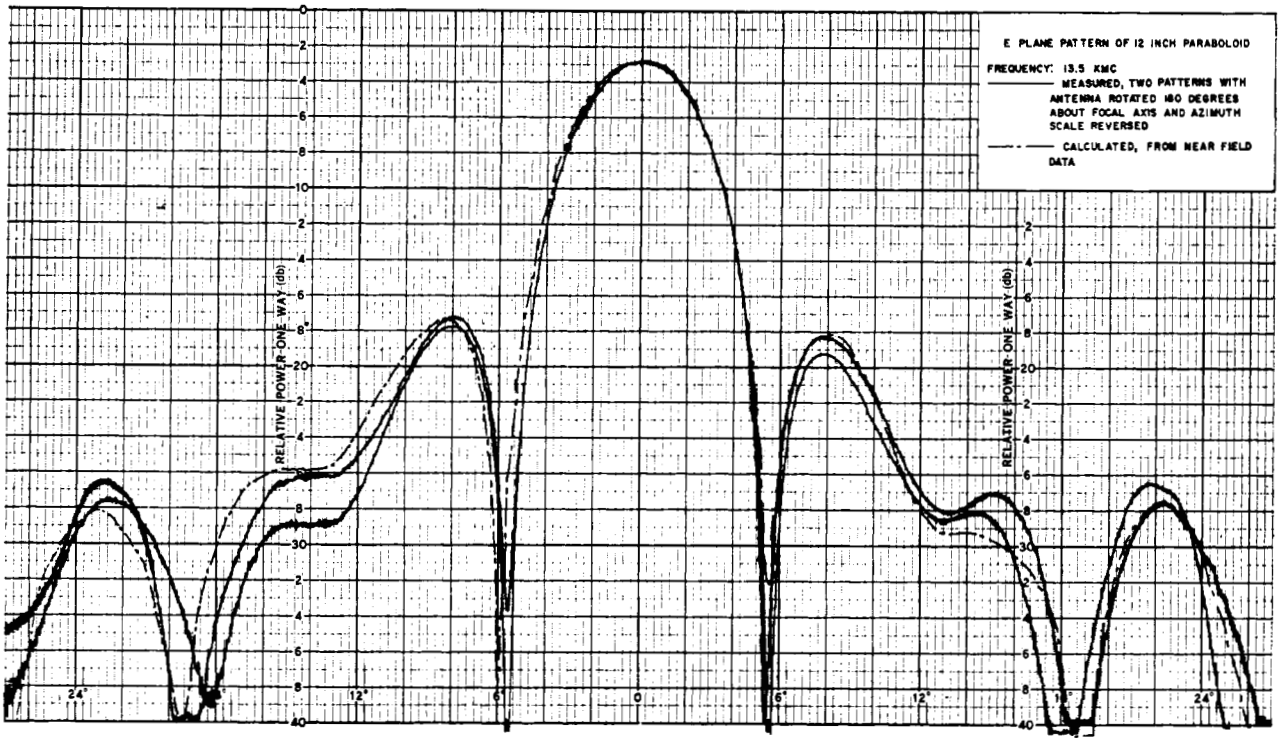

Fig. 7. Measured and computed E-plane patterns of a 30.5-cm paraboloidal antenna operating at 13.5 GHz. Two measured patterns are shown with the antenna rotated 180° about its focal axis between the two measurements.

over a 40-dB dynamic range. The phase and amplitude of the aperture field were measured along H-plane cuts made at intervals of 1.27 cm over a 50.8-cm square located about 25 cm in front of the dish. The near-field probe was a dielectrically loaded waveguide with inside dimensions of 0.57 cm by 0.28 cm.

A principal E-plane pattern was calculated from these data using an analog type Fourier integral computer described by Clayton and Hollis [32]. This computer applies the scalar diffraction integral given in (13) with previously defined approximations for far-field calculations.

A comparison of measured and calculated E-plane patterns for the 30.48-cm paraboloidal antenna is given in Fig. 7. Two measured patterns are shown because the far-field patterns were measured on a temporary range with relatively large unwanted reflections. The antenna was rotated through 180° about its focal axis between measurements of the two patterns as an indication of the interference resulting from range reflections. Very good agreement between the measured and calculated patterns is achieved considering the variation in the two measured patterns due to reflections.

As indicated by the preceding examples, the source distribution method can be used to calculate far-field patterns with acceptable accuracy for the main beam and close-in sidelobes. Probes, near-field positioners, and receiving systems using phase-lock techniques are now available that permit simultaneous phase and amplitude measurements of near fields with greater accuracy than indicated above. With measurement data from such systems, the scalar diffraction integral is adequate for many situations. Although better agreement between measured and calculated results can be achieved with a vector formulation of the diffraction integral, the modal expansion method presented in the next section is superior to both the scalar and vector diffraction integral methods.

Far-Field Determination by the Modal Expansion Method

Basic Concepts: In the modal expansion method, measured near-field data from an antenna are converted to a summation or spectrum of modes corresponding to wavenumbers in the coordinate system in which the near-field data are measured. The pattern of the probe is also transformed to obtain a modal expansion in terms of wavenumbers. With these data the weighting of the probe pattern on each component of the wavenumber spectrum of the near-field data can be eliminated on a term-by-term basis. This corrected wavenumber spectrum can then be used to obtain the far-field pattern for the test antenna. Thus one of the major difficulties in applying the source distribution method to determine far-field patterns, that of finding an ideal probe for measurement of the source distribution, is eliminated by the modal expansion method.

The modal expansion method is based on the fact that an arbitrary electromagnetic field pattern can be expressed as a linear combination of a set of orthogonal solutions in an appropriate coordinate system. Booker and Clemmow [33] analyzed the concept of a spectrum of plane waves in terms of the relationship between an aperture distribution and the polar antenna pattern. They derived the relationship between the near field of an aperture antenna and the plane-wave expansion and the conditions under which the plane-wave spectrum can be expressed in terms of the far-field polar antenna pattern.

Kerns [34] and Dayhoff [35] have used the plane-wave modal expansion method to eliminate the effects of probe characteristics in determining far-field patterns from near-field measurements. For the special case of no multiple reflections between test antenna and probe, they developed a method to eliminate the effects of the probe characteristics on the calculated far-field pattern. This work utilized a scattering matrix analysis and could be applied to arbitrary an-

tennas and probes if the pattern characteristics of the probe were known.

Joy and Paris [36] have investigated sample spacing criteria and techniques to minimize required near-field measurement data in the determination of far-field patterns from near-field measurements using the plane-wave modal expansion method. Two-dimensional spatial filtering was used to reduce the computations required to calculate far-field patterns. Also, the plane-wave spectrum of near-field data was corrected for the effects of the measurement probe.

A two-dimensional cylindrical-wave modal expansion technique has been investigated by Brown [37], [38] and Jull [38]–[40] and results have been experimentally verified. They treated a cylindrical line source to obtain full 360° patterns around the antenna. However, their work was limited to two-dimensional problems for which there is no dependence on the z coordinate. A method for compensating for the effects of the probe was developed and shown to be practical if the wavenumber spectrum of the probe were known.

Leach [41] has developed a new method for determining the far-field pattern of an antenna from probe-compensated near-field measurements over the surface of a right circular cylinder enclosing the antenna. This method is derived by expanding the radiated near field in cylindrical-wave expansions and by using the Lorentz reciprocity theorem to solve for the fields radiated by the antenna. The problem of spatial sampling criteria is also treated for the cylindrical measurement surface and lower bounds are established for the axial and polar angle sample interval on the cylinder.

Jensen [42] has described a method for obtaining a far-field pattern from measurements of the near field over a sphere that encloses the test antenna. A procedure for compensating for the characteristics of the probe is described also, although neither the basic technique nor the compensation method have been tested experimentally. Ludwig [43] uses a spherical-wave expansion as a numerical technique for expressing arbitrary fields specified by analytical, experimental, or numerical data. The application of this technique, however, was for the computation of near-field patterns from far-field data and Ludwig shows comparisons of measured and computed patterns that demonstrate the accuracy of the technique.

James and Longdon [44] have described a method for obtaining the far-field spherical-wave expansion of an arbitrary antenna from measurements of the radial component of the electric and magnetic fields over a sphere enclosing the antenna. A disadvantage of this method is the rapid rate at which the radial fields decrease with distance from the antenna. In addition, the method requires the use of two measurement probes, one for the electric field and one for the magnetic field. No technique for probe compensation was described in their investigation.

Plane-Wave Expansion: The function known as the wavenumber spectrum for a plane-wave expansion can be derived from the tangential components of the electric field vector $\boldsymbol{E}$ over the plane aperture of interest. Thus if the aperture is located in the plane $z=0$, the plane-wave spectrum can be expressed as

$$\boldsymbol{A}(k_x, k_y) = \frac{1}{2\pi}\int_{-\infty}^{\infty}\int_{-\infty}^{\infty} \boldsymbol{E}(x, y, 0) \exp\left[-j(k_x x + k_y y)\right] dx dy \quad (17)$$

where k_x and k_y are the wavenumbers in the x and y directions, respectively. As shown by Clemmow [45], the electric field intensity in the charge-free region $z \geqq 0$ can be represented as

$$\boldsymbol{E}(x, y, z) = \frac{1}{2\pi}\int_{-\infty}^{\infty}\int_{-\infty}^{\infty} \boldsymbol{A}(k_x, k_y) \exp\left[j\boldsymbol{k}\cdot\boldsymbol{R}\right] dk_x dk_y \quad (18)$$

where

$$\boldsymbol{k} = \hat{a}_x k_x + \hat{a}_y k_y + \hat{a}_z (k_0^2 - k_x^2 - k_y^2)^{1/2}$$
$$k_x^2 + k_y^2 \geq k_0^2 \quad (19)$$

and $k_0 = 2\pi/\lambda$ is the free space wavenumber. Although the evaluation of the integral in (18) may not be possible in the general case, for $k_0 z \gg 1$ an asymptotic expansion for the electric field in the far-field region can be derived by the method of steepest descent and represented as

$$\boldsymbol{E}_f(R, \theta, \phi) = \frac{jk \cos\theta e^{-jk_0 R}}{R} \boldsymbol{A}(k_{x0}, k_{y0}) \quad (20)$$

where the wavenumbers k_{x0} and k_{y0} are the values of k_x and k_y at the saddle point of the integral given in (18). These saddle point values are given by

$$k_{x0} = k_0 \sin\theta \cos\phi$$
$$k_{y0} = k_0 \sin\theta \sin\phi. \quad (21)$$

Joy and Paris [36] have established the sample spacing criterion for field samples over a rectangular lattice in the plane separated by grid spacings Δx and Δy. If it is known that the plane-wave spectrum is zero for $|k_x| \geqq k_{xm}$ and $|k_y| \geqq k_{ym}$ where k_{xm} and k_{ym} are positive real numbers, then the electric field can be reconstructed for all points on the plane $z=0$ with grid spacings of $\Delta x = \pi/k_{xm}$ and $\Delta y = \pi/k_{ym}$. If the measurement plane $z=0$ is located in a region which contains no evanescent waves, then the maximum wavenumbers are $k_{xm} = k_{ym} = k_0 = 2\pi/\lambda$. For this case, the maximum sample spacings for the field are $\Delta x = \Delta y = \lambda/2$.

Burns, Joy, and Rodrigue at Georgia Tech have recently completed a comparison of far-field patterns computed by the plane-wave expansion method from near-field measurement data with patterns measured directly on far-field ranges. For this investigation, the test antenna was a 1.22-m paraboloid operated at 5.45 GHz with an azimuth (only) monopulse feed. The near field of the antenna was sampled at spacings of $\lambda/3$ in a plane approximately 10λ from the antenna aperture. Measured near-field amplitude and phase distributions for a 128 by 128 matrix of measurement points in a plane parallel to the aperture are shown in Figs. 8 and 9 for the monopulse difference pattern. The near-field phase distribution shows clearly the 180° difference in phase between the two lobes of the difference pattern and also the circular region corresponding to the collimated beams that is approximately the size of the aperture. The interfering field due to back radiation and diffraction from the feed produces concentric circular ridges in both the phase and amplitude plots.

The near-field data shown in Figs. 8 and 9 were used to compute the far-field difference pattern of the test antenna. Fig. 10 shows a three-dimensional representation of this computed pattern in wavenumber space for an angular sector ±22° in azimuth and in elevation. Fig. 11 shows a comparison of the principal azimuth plane pattern calculated by the plane-wave expansion method from near-field data with the pattern from the same plane measured on a far-field range.

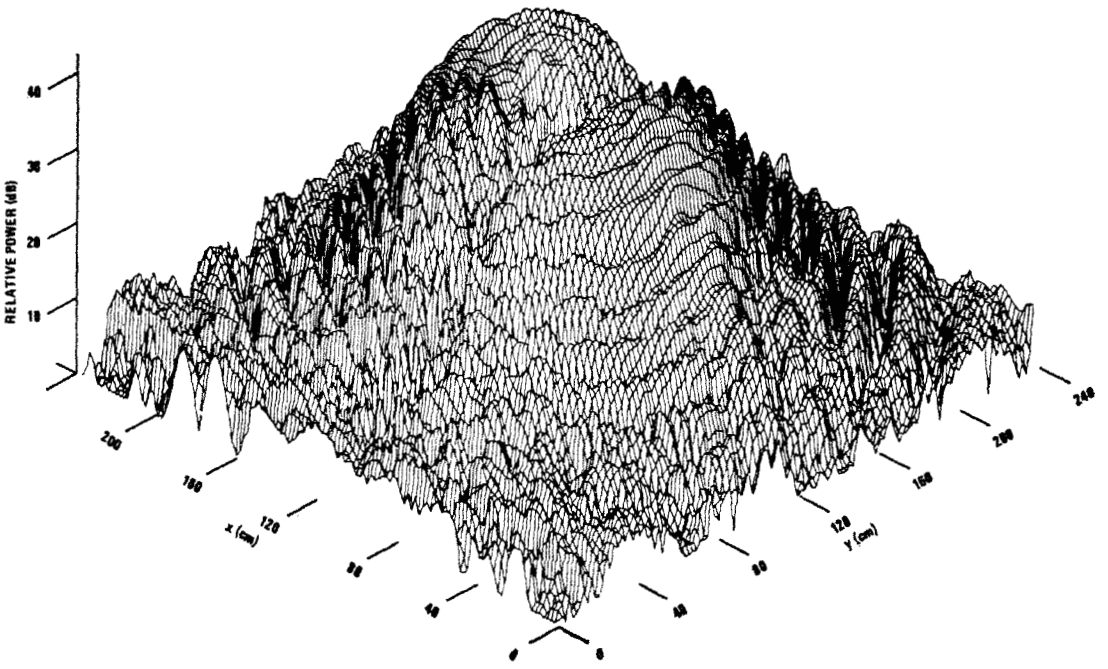

Fig. 8. Near-field amplitude distribution for azimuth (only) monopulse antenna. *Difference* pattern at 5.45 GHz.

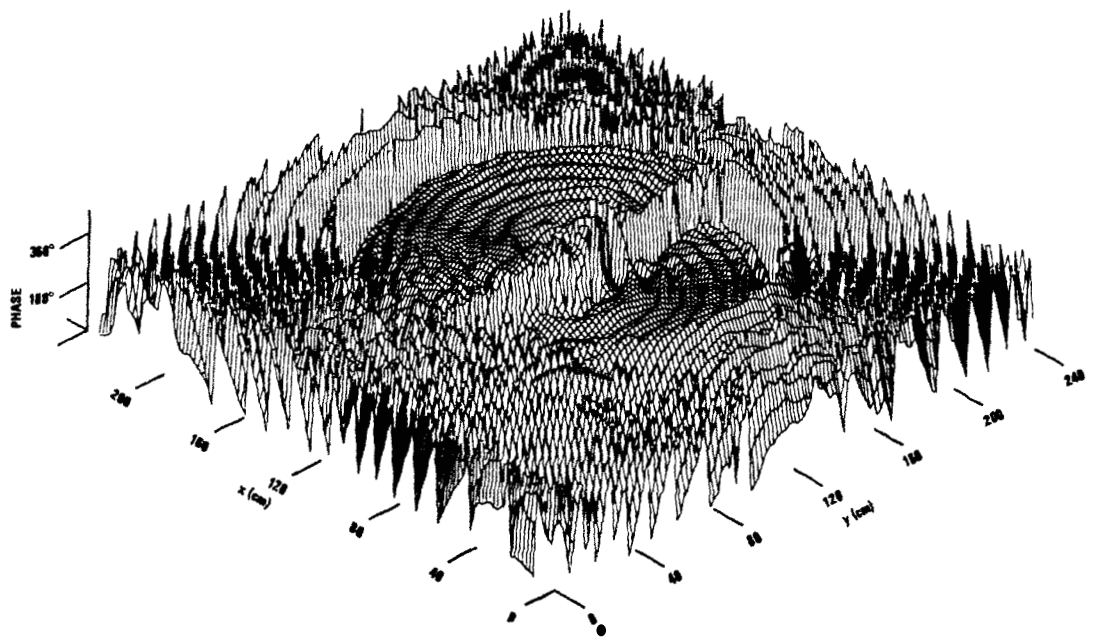

Fig. 9. Near-field phase distribution for azimuth (only) monopulse antenna. Difference pattern at 5.45 GHz.

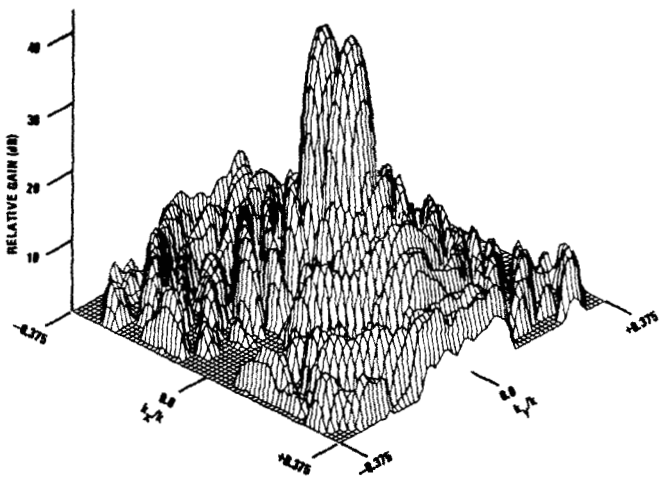

Fig. 10. Computed far-field difference pattern in wavenumber space for azimuth (only) monopulse antenna operating at 5.45 GHz. Along each principal plane ($k_x = 0$ or $k_y = 0$), the angular section is approximately $\pm 22°$.

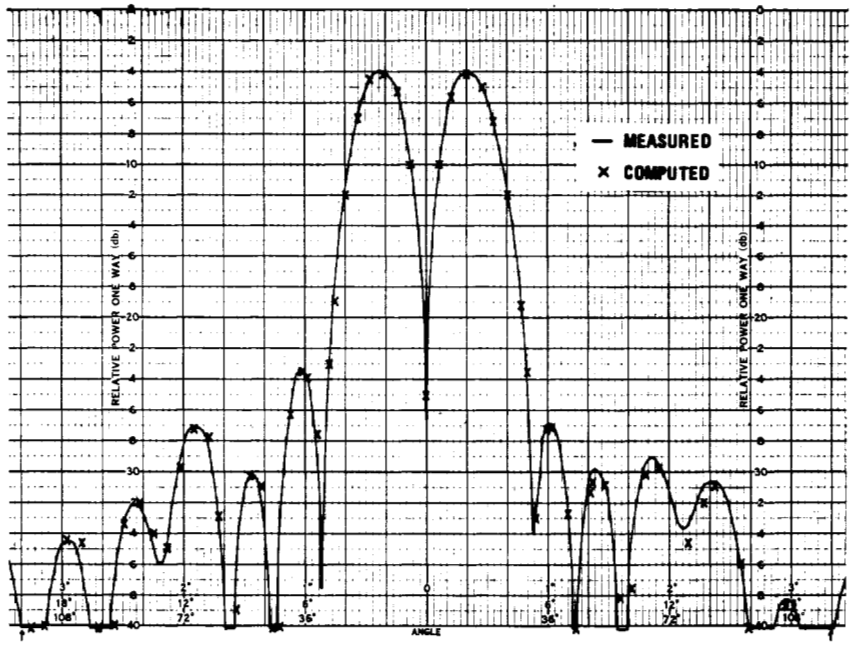

Fig. 11. Comparison of measured far-field pattern and computed far-field pattern over a ±20° sector in principal azimuth plane of monopulse difference pattern at 5.45 GHz.

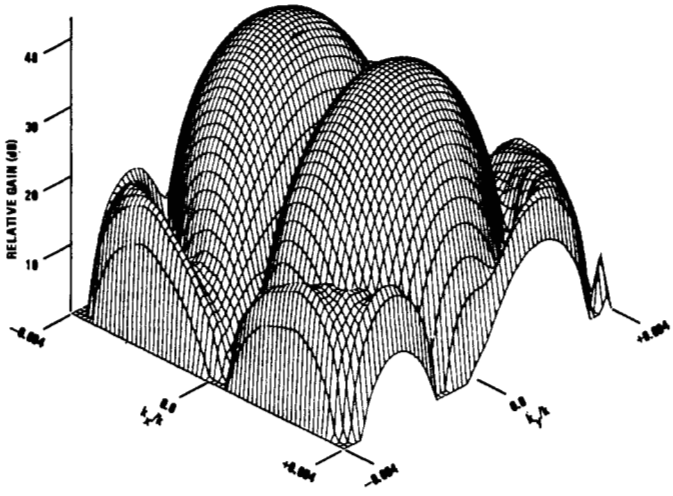

Fig. 12. High-resolution plot of main-beam region of computed far-field pattern in wavenumber space for azimuth (only) monopulse antenna operating at 5.45 GHz. Along each principal plane ($k_x = 0$ or $k_y = 0$), the angular sector is approximately ±5°.

Computer capacity determines the resolution with which the pattern can be calculated for any given angular sector. If better resolution is required, the pattern can be divided into subsectors and calculations can be made for each subsector separately. For example, Fig. 10 shows a pattern for an angular region of ±22° plotted from a 63 by 63 matrix of computed points. If only the main beam region ±5° from the difference null is of interest, the same number of points can be computed for the reduced sector resulting in increased resolution as shown in Fig. 12.

Recent work at the National Bureau of Standards by Baird, Newell, Wacker, and Kerns [46] also substantiates that very accurate determinations of far-field radiation patterns and gain are possible with the modal expansion method using the plane-wave spectrum technique. Operating at 47.75 GHz over a dynamic range of 45 dB, they investigated the plane-wave spectrum of an open-ended waveguide, a standard gain horn, and an electrically large horn-lens antenna. It is their opinion that because of the rigorous theoretical structure and the experimental documentation that the calculated far-field results obtained by applying the modal expansion method to near-field measurements are at least as accurate and as easily obtained as any results of equal completeness that could be obtained from direct far-field measurements.

Cylindrical-Wave Expansion: It can be shown that the cylindrical-wave spectrum of an antenna can be obtained from the output of a probe used to measure the tangential electric field on the surface of a right circular cylinder enclosing the antenna. The cylindrical-wave spectrum of the probe can be used to modify the measured results from the test antenna to compensate for the nonideal characteristics of the probe. When the method of steepest descent is applied to approximate the far field of the cylindrical-wave spectrum, Leach [41] shows the result is

$$E_R = 0$$

$$E_\theta = \frac{-j2\sin\theta}{R} e^{-jk_0R} \sum_{n=-\infty}^{\infty} j^n b_n(k_0\cos\theta) e^{jn\phi}$$

$$E_\phi = \frac{-2\sin\theta}{R} e^{-jk_0R} \sum_{n=-\infty}^{\infty} j^n a_n(k_0\cos\theta) e^{jn\phi} \qquad (22)$$

in which $a_n(k_0\cos\theta)$ and $b_n(k_0\cos\theta)$ are the amplitude weighting functions of the cylindrical-wave vector expansion and k_0 is the free space wavenumber. As shown by Leach [41], the values of these amplitude weighting functions can be derived from the output of the probe for two orthogonal polarizations and from the sets of clylindrical amplitude weighting functions that represent the radiation pattern of the probe for two orthogonal polarizations. Thus the resulting cylindrical-wave spectrum for the test antenna is determined with compensation for the effects of the probe.

Leach [41] has shown that the sample spacing criteria in azimuth angle ϕ and axial direction z for near-field measurements on a right cylindrical surface are

$$\Delta\phi = \frac{\pi}{N} \tag{23}$$

and

$$\Delta Z = \frac{\pi}{k_0} \tag{24}$$

where N must be chosen as the smallest integer greater than k_0a and a is the radius of the smallest cylinder completely enclosing the antenna.[3] If the value of k_0 is substituted into the above expressions with $N = k_0a$, the sample spacings become

$$\Delta\phi = \frac{\lambda}{2a} \tag{25}$$

and

$$\Delta Z = \frac{\lambda}{2}. \tag{26}$$

Note that the arc length on the cylinder separating adjacent sample points on the smallest cylinder enclosing the antenna is

$$\Delta S = a\Delta\phi = \frac{\lambda}{2}. \tag{27}$$

Leach constructed a slotted waveguide array as a test antenna for the cylindrical-wave expansion technique. The array of slots was cut into the broad wall of a 43.7-cm length of WR 90 waveguide. Ten slots resonant at 9.68 GHz were located alternately approximately 0.25 cm from the centerline of the guide. For the near-field measurements, the slotted array was mounted vertically and the probe was set at a radius of 30.5 cm from the test antenna. The cylinder was divided into 32 vertical scans of the probe, each separated by 11.25° in the azimuthal angle ϕ_0. The length of each scan on the cylinder was approximately 132 cm.

Fig. 13 shows a comparison of measured and calculated far-field patterns of this test antenna for the cylindrical modal expansion method. Principal plane cuts for both elevation and azimuth patterns are shown. Unfortunately, the measurements of the probe pattern and the near-field measurements from the test antenna were made in an environment in which stray radiation was relatively high. Although good agreement is shown over most angular regions in both principal planes, it is felt that much better agreement would be possible if stray radiation and reflections in the vicinity of the near-field range could be reduced. For all measurements and computed elevation patterns, there was disagreement in the region between 35° and 65°. There appears to be strong evidence that this disagreement can be traced to reflections from the surroundings that occurred during measurements.

Spherical-Wave Expansion: The solutions to the homogeneous vector-wave equations in spherical coordinates are well known and are discussed in detail by Stratton [8, ch. 7]. The vector-wave solutions include the vector-wave functions M_{mn} and N_{mn} that are required to describe the complex $\boldsymbol{E}$ and $\boldsymbol{H}$ fields of families of transverse-electric (TE) and transverse-magnetic (TM) waves. These vector-wave functions are given in terms of the polar angle θ, the azimuthal angle ϕ, and the radius R and their associated unit vectors. In addition to the harmonic functions, sine and cosine, the associated Legendre polynomials of the first kind and spherical Bessel functions are necessary to describe the spherical-wave solutions. For the spherical wave to satisfy the radiation condition at infinity, the spherical Bessel functions are restricted to spherical Hankel functions. Potter [47] has investigated the properties of these spherical-wave functions and discusses in detail the approximations that are valid in the various field regions.

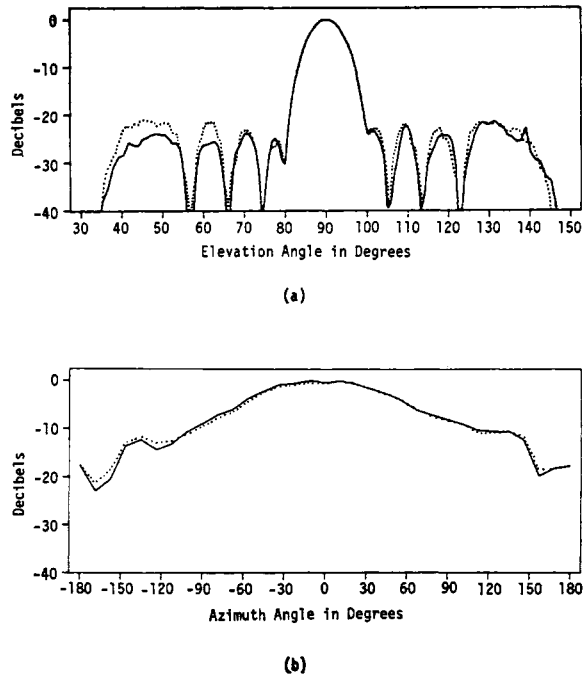

Fig. 13. Measured and calculated far-field E- and H-plane patterns of a 43.7-cm slotted waveguide array antenna operating at 9.68 GHz. The calculated patterns were obtained by the cylindrical-wave model-expansion method. (From Leach, [41].) (a) Elevation pattern of E_ϕ: solid line, calculated; dotted line, measured. (b) Azimuth pattern of E_ϕ: solid line, calculated; dotted line, measured.

Ludwig [43] shows that both the electric and magnetic fields can be expressed as summations of the spherical-wave functions and that the coefficients of these wave functions can be derived from the tangential electric field alone on a sphere of radius $R_1 > R_0$. (A sphere of radius R_0 contains all sources.) In terms of the spherical-wave functions and their coefficients, the fields for $R > R_1$ can be expressed as

$$E(R, \theta, \phi) = -\sum_m \sum_n a_{mn}M_{mn} + b_{mn}N_{mn} \tag{28}$$

$$H(R, \theta, \phi) = (k/j\omega\mu) \sum_m \sum_n a_{mn}M_{mn} + b_{mn}N_{mn} \tag{29}$$

where the coefficients a_{mn} and b_{mn} are those derived by Ludwig from the tangential electric field on the surface of a sphere. Because all sources were defined to be within the sphere of radius R_0, spherical waves of order $n > kR_0$ will not contribute significantly to the field [47]. Thus the series can be truncated and the coefficients derived for a finite number of terms in the expansion. The expansion can then be developed to express the total electromagnetic field everywhere outside the sphere of radius R_1.

Only limited experimental verification has been accomplished for the spherical modal expansion. The majority of the

[3] The actual near-field measurements do not have to be made on the cylinder of smallest radius; consequently, measurements at incremental arc lengths greater than $\lambda/2$ yield an advantage in data reduction.

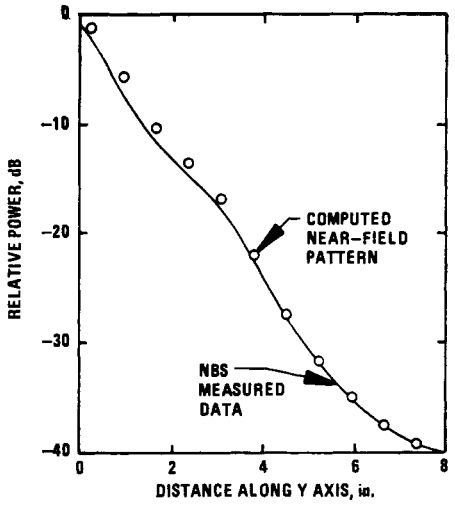

Fig. 14. Comparison of measured and computed near-field patterns of a conical feed horn. The spherical-wave modal-expansion method was used to calculate the near-field pattern. (From Ludwig, [43].)

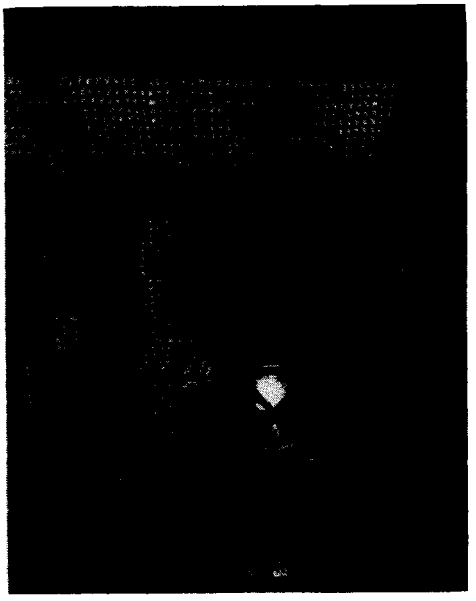

Fig. 15. Front view of near-field probe and x–y–z positioner.

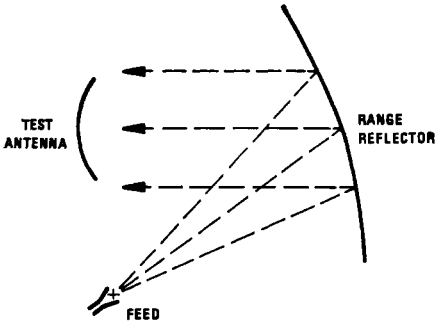

Fig. 16. Schematic representation of a compact range employing a reflector and feed.

work has been in the development of design techniques for Cassegrainian-fed paraboloids. For this application, the spherical modal expansion method is used to transform far-field patterns of feeds to near-field patterns. The process is essentially the same as for the inverse transformation and is valid if the sphere in the near field is of sufficient radius to preclude the existence of evanescent waves of significant amplitude in the region of the surface of the sphere. In Fig. 14 a comparison of measured and computed near-field patterns made by Ludwig [43] using the spherical modal expansion method is shown. The test antenna was a conical feed horn with a 3-dB beamwidth in both the E and H planes of approximately 1.5°. The near-field radiation of the horn was measured by the Bureau of Standards in a plane about 20.3 cm in front of the aperture. The computed near field by Ludwig shows excellent agreement with the measured pattern.

Modal Expansion Implementations: Of the three geometries in which the modal expansion method has been investigated, the plane-wave spectrum in rectangular coordinates has received the most attention. Currently, most of the very accurate near-field probe positioners are designed to permit movement of the probe in an x–y plane parallel to the aperture of the antenna as shown in Fig. 15. Positioning in the z direction is accomplished by movement of the test antenna. The only significant microwave absorber requirements are in the area of the main beam of the test antenna.

Probing in a cylindrical coordinate system can be accomplished using a near-field probe capable of scanning vertically and a conventional antenna pedestal capable of azimuth rotation. The test antenna is rotated in azimuth by fixed angular increments and at each azimuth position the probe is scanned vertically, the z direction in the cylindrical coordinate system. Accurate measurements in the cylindrical coordinate system require an outdoor range or an anechoic chamber because the main beam is rotated in the measurement procedure and reflections from surroundings will affect the near-field measurements.

A conventional two-angular coordinate antenna positioner could be used to obtain measurements in the near field for the spherical coordinate system. However, as in the cylindrical coordinate system, an anechoic chamber or free-space conditions must be available to reduce reflections. As mentioned previously, only limited experimental results have been obtained using the spherical modal expansion method.

Recent results indicate that the near field of microwave antennas can be measured with sufficient accuracy to produce accurate far-field patterns by application of modal expansion methods. The characteristics of the near-field probes are not critical because they can be eliminated from the final results. In addition, accurate gain determination can be made from the near-field data. Care must be taken in the near-field measurements to minimize reflections from the surroundings and to accurately locate the position of the measurement probe at each sampling point. When low-sidelobe antennas are involved, the near-field measurements must be made over a sufficiently large dynamic range to provide the information necessary to describe these sidelobes.

Compact Ranges

As stated earlier, the testing of microwave antennas usually requires that the antenna be illuminated by a uniform plane electromagnetic wave. In compact ranges, the incident wave is created by a reflector or lens close to the antenna under test

Fig. 16 is a schematic representation of a compact range which employs a large reflector (designated the range reflector) with feed. The diverging rays from the feed are collimated by

the range reflector, and the test antenna is located in the collimated beam near the reflector. In this manner, far-field results can be obtained.

Background

The advantages of having laboratory methods for measuring antenna patterns indoors were recognized many years ago. Most of the early attempts used lenses as the collimating device, but later attempts used reflectors.

Woonton, Borts, and Carruthers [48] conducted X-band compact-range experiments using metal-plate lenses as collimating devices. Trials with a stepped lens of 35 wavelengths square aperture were not successful, and the failure was attributed to the diffraction effects caused by the steps. An unstepped lens of rectangular aperture 35 by 7 wavelengths proved more successful over a limited angular range; however, the performance of the measurement range was limited by diffraction from the edges of the collimating lens.

The errors arising in the measurement of antenna patterns by means of a collimating lens later were examined theoretically by Woonton, Carruthers, Elliot, and Rigby [49]. They found that the errors can be reduced by increasing the size of the collimating lens, and they predicted that a large lens, 40 wavelengths in diameter, may be used for the precision measurement of the pattern of any radiating aperture of dimensions not less than 10 wavelengths and not more than 20 wavelengths over an angular interval that includes the second sidelobe.

Some experimental investigations were made by Chapman [50] using a solid polystyrene aplanatic lens. The collimating lens was 35 wavelengths in diameter and the two test horns whose patterns were studied had rectangular apertures with a maximum dimension of 15 wavelengths or less. Unfortunately, the indoor measurements showed large errors when compared to outdoor measurements on a far-field range. Reflections at the surface of the collimating lens probably contributed largely to the failure of the indoor range.

In later work, Mentzer [51] used a dielectric lens of low dielectric constant to collimate a beam for measuring radar cross sections of various targets. The lens was 33 wavelengths in diameter, and it was constructed of styrofoam having a dielectric constant of about 1.03. Using material with such a low dielectric constant reduced reflections at the lens surfaces to an acceptable level; however, a large focal length was required ($f/D \approx 10$). The use of such a lens reduces the required length of the measurement range, but the long focal length tends to disqualify such a range from being described as "compact."

Some investigations were reported by Crysdale [52] in which antenna patterns were measured using a large paraboloidal reflector as the collimating device. Large errors were found, and methods of reducing these were discussed; however, the observations were incomplete and inconclusive.

Kay [53] considered the question of what is the minimum required separation between transmitting and receiving antennas for far-field measurements, and then he explored techniques whereby true far-field patterns may be measured at closer distances. Kay's theoretical considerations led to the conclusion that if the probe (transmitting) antenna has a larger aperture than the antenna under test and the phase and amplitude are uniform over the aperture of the probe antenna and if interaction effects are neglected, then the far-field pattern of the test antenna may be taken at short distances up to physical contact with the probe antenna.

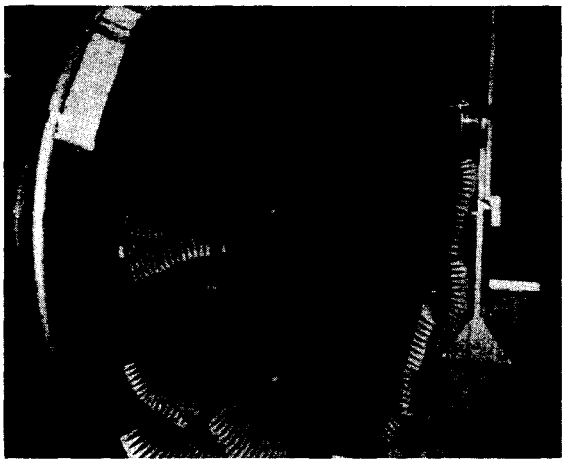

Fig. 17. Photograph of a point-source compact range with a paraboloidal reflector test antenna in position.

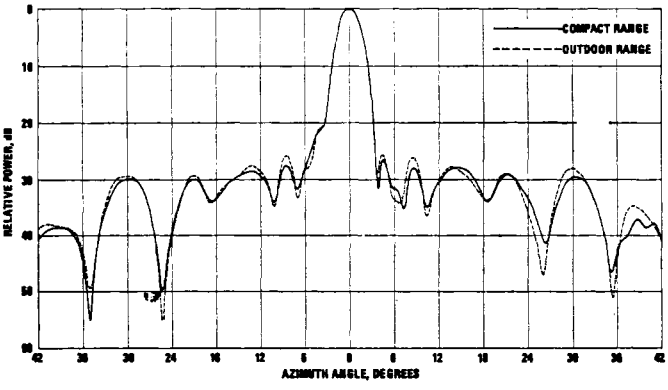

Fig. 18. Comparison of azimuth patterns (H plane) measured on a point-source compact range and on a far-field outdoor range. The antenna was a 76-cm paraboloidal reflector with a horn feed operating at 10 GHz.

Johnson *et al.* [54]–[58] later demonstrated that far-field measurements with full-size antennas can be made on indoor compact ranges using reflectors. Two range configurations were constructed; one was a line-source range consisting of a parabolic-cylinder reflector with a large hoghorn [59] feed, and the other was a point-source range consisting of a paraboloidal reflector with a small horn feed.

The line-source range has the advantages of being easy to construct accurately and of producing a pure linear polarization because of the cylindrical reflector; however, there are some serious disadvantages. Such a range, in practice, is limited to a single linear polarization and it is difficult to change frequency bands. To illustrate the latter difficulty, for any large change in frequency it is necessary to alter the physical size of the line-source aperture of the hoghorn in the plane normal to the direction of the reflector focal line. This difficult alteration is necessary to maintain proper illumination over the aperture of the parabolic-cylinder reflector.

The point-source range is much more versatile. The polarization is determined essentially by the characteristics of the feed, and the reflector is useful over a wide band of frequencies. The upper frequency limit is determined by surface deviations (from a true paraboloidal shape), and the lower frequency limit is determined by diffraction effects from the edges of the range reflector. A properly designed and fabricated range should be useful over several waveguide frequency bands.

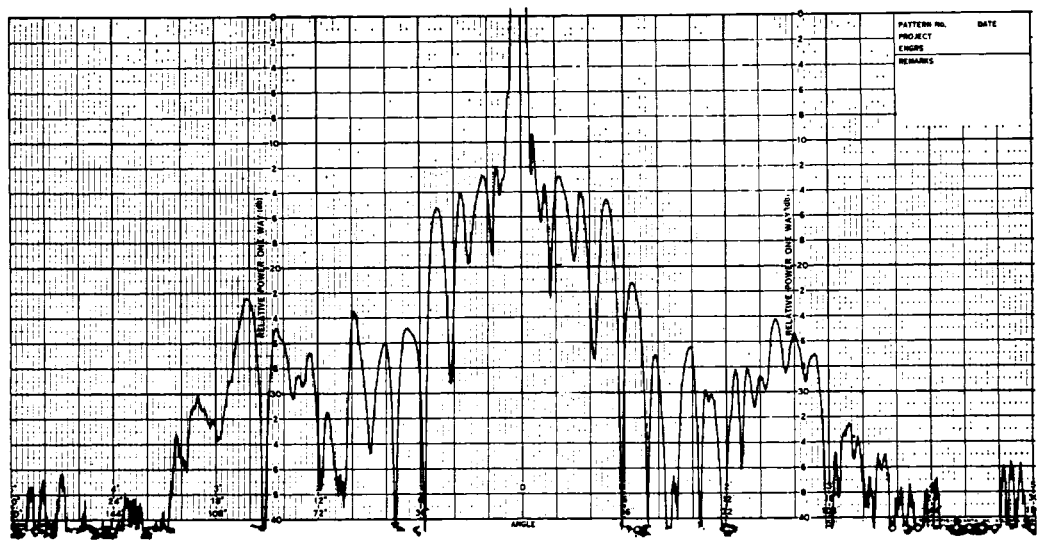

(a)

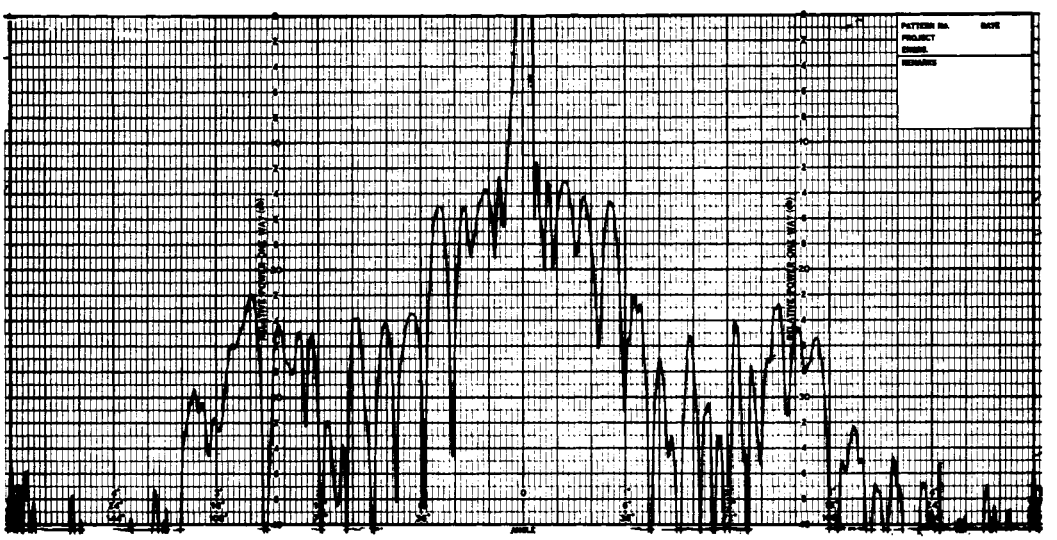

(b)

Fig. 19. Azimuth patterns (*H* plane) measured on a far-field outdoor range and on a point-source compact range. The antenna was a 76-cm paraboloidal reflector with a horn feed operating at 10 GHz. The gain level at the top of each chart is −15 dB relative to the peak of the main lobe. (a) Outdoor range. (b) Compact range.

Fig. 17 is a photograph of an experimental point-source range. It consists of a 3-m paraboloidal range reflector which is illuminated by an open-ended waveguide surrounded by a pyramidal horn in which the internal walls are lined with absorbing material. This absorbing material reduces wide-angle radiation from the open-waveguide feed. Additional absorbing material is located below the feed to further reduce back radiation and diffraction from the feed supports, and some absorbing material is located around the periphery of the upper half of the reflector to reduce the effects of edge diffraction.

The test antenna shown in Fig. 17 is a 76-cm paraboloidal reflector with an *X*-band horn feed. Patterns of the test antenna were recorded on the point-source range and then compared with patterns recorded on a far-field outdoor range. A typical comparison of expanded scale patterns is illustrated in Fig. 18, and a typical comparison of 360° patterns is illustrated in Fig. 19. Note the close agreement between patterns recorded on the outdoor and compact ranges.

Design of New Ranges

The experience gained by working with early models of compact ranges makes it possible now to design and fabricate improved ranges. The several problem areas which must be considered in the design of compact ranges are listed below, and they will be discussed in the remainder of this section:

1) direct radiation from the feed,
2) diffraction from feed and supports,
3) diffraction from reflector edges,
4) depolarization,
5) space attenuation from primary feed,
6) interaction between range and test antenna.

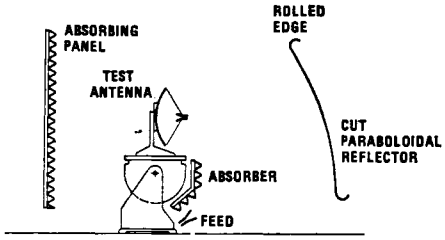

Fig. 20. Schematic diagram of an improved point-source compact range.

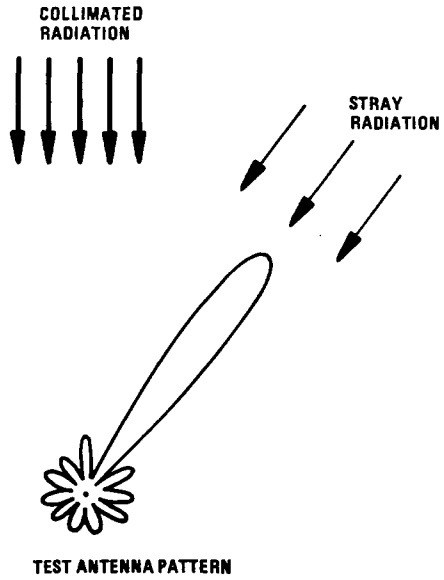

Fig. 21. Sketch depicting a situation in which the main lobe of the test antenna is directed toward a stray radiation source while a sidelobe is directed toward the collimated radiation.

7) stray radiation within room,
8) reflector surface tolerances.

Before discussing the above problem areas, consider the schematic diagram of an improved point-source compact range which is illustrated in Fig. 20. The range reflector is a cut paraboloid with an offset feed, the focal length is fairly long, and the feed is located essentially underneath the antenna positioner. The collimated beam passes from the reflector to the absorbing panel, and the test antenna is immersed in this collimated beam.

In addition to the collimated radiation there is stray radiation which adds both in and out of phase with the collimated energy and hence perturbs the desired plane incident wave. Such stray radiation can degrade the accuracy of antenna pattern measurements, so efforts must be made to reduce its effects. Fig. 21 depicts a situation in which the main lobe of the test antenna is directed toward a stray radiation source while a sidelobe is directed toward the collimated radiation. Note that the contribution of the stray radiation relative to the contribution of the collimated radiation is increased by the ratio of the gains of the main and side lobes. One can see that, in order to accurately test high-gain low-sidelobe antennas, it is necessary to keep stray radiation below acceptable levels. The effects of stray radiation on a compact range are no different than those on an outdoor far-field range, but the sources of stray radiation are different on the two ranges.

Direct Radiation from Feed: Direct radiation from the feed to the test antenna can be a source of serious problems; however, it can be reduced to an acceptable level by designing a feed with low radiation in the direction of the test antenna and by placing high-quality absorbing material in a position to intercept the radiation, as illustrated in Fig. 20.

Diffraction from Feed and Supports: The use of a cut paraboloid with an offset feed greatly reduces the amount of energy incident on the test antenna after being diffracted or scattered by the feed and supports, because the main beam of collimated energy passes above the feed. Such diffracted or scattered energy can be reduced further by locating the test antenna essentially over the feed and by placing absorbing material between the feed and the test antenna.

Diffraction from Reflector Edges: Discontinuities at the edges of the range reflector interrupt the normal flow of currents and produce stray radiation not in phase with the collimated radiation. This stray uncollimated energy can be greatly reduced by "rolling" the edge of the reflector. In effect, this relocates the sharp diffraction edge from the front of the reflector to a less exposed region behind the reflector.

Normally, the larger the radius of curvature (of the roll) the better; however, the size and weight of the reflector increase also, so a practical radius must be selected. By estimating backscatter from cylindrically curved edges with various radii and terminations, Ryan [60] suggested that the radius of curvature be one wavelength or greater at the lowest operating frequency with an arc length of about 180° or greater.

Depolarization: The primary field radiating from the point-source feed has certain polarization characteristics which depend on the type of feed which is employed; however, when this primary field is reflected by the doubly curved paraboloidal reflector, a cross-polarized component can be generated. The magnitude of the cross component will depend on the reflector geometry, but it will be small near the reflector axis and it will decrease with increasing focal length. Thus for a given aperture, a long focal length is desirable to reduce depolarization effects to an acceptable level.

Space Attenuation: The energy radiating from the feed and traveling toward the range reflector moves with essentially a spherical wavefront. After reflection, the energy is collimated and moves with essentially a plane wavefront.

While the energy is diverging between the feed and the reflector, the power density (in watts per square meter) decreases as the square of the distance from the feed; however, after collimation the power density remains essentially constant. The distance from the focal point to a paraboloidal reflector increases with the angle from the axis. Thus if such a reflector were illuminated by an isotropic source, the collimated beam would have the greatest power density along the axis, and the power density would decrease with distance from the axis.

For a given size reflector (aperture), the space-attenuation effect will decrease with increasing focal length, so it is advantageous to have a long focal length on a compact range. In addition, the feed can be aimed toward the top edge of the reflector so that the taper of the feed pattern tends to nullify the space attenuation.

Fig. 22 illustrates the power-density distribution which was measured by moving a small probe antenna vertically through the test volume of a line-source range, and Fig. 23 illustrates the power-density variation which was measured by moving a small probe antenna axially away from the range reflector of a line-source range. These figures demonstrate that a uniform field intensity can be realized within the test volume of a compact range.

Interaction: When transmitting and receiving antennas

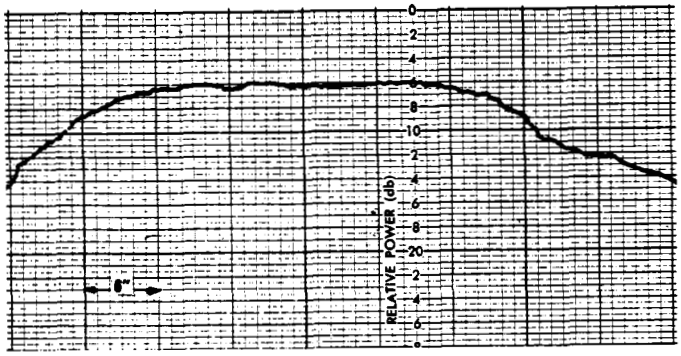

Fig. 22. Power density distribution with vertical polarization at 10 GHz for a vertical cut in the test volume of a line-source compact range.

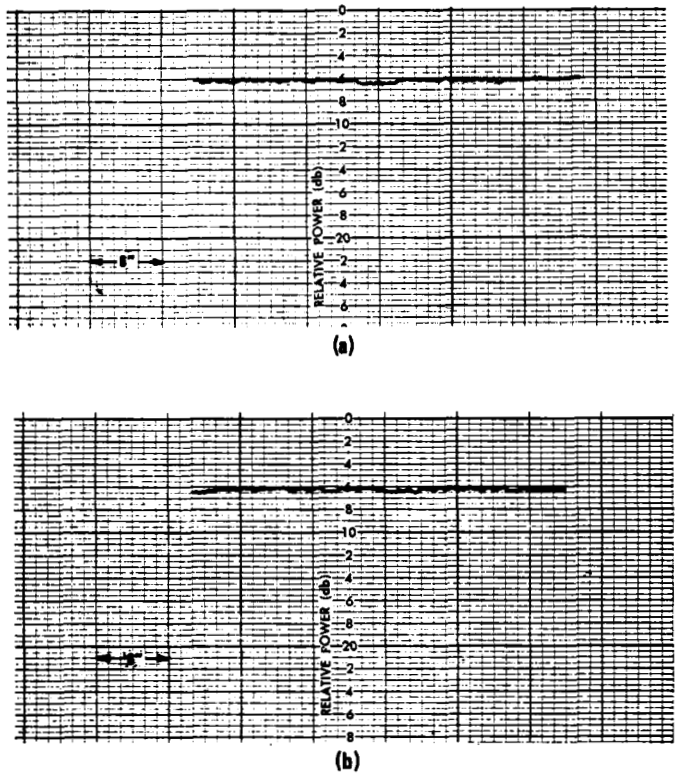

Fig. 23. Power density variation with distance from range reflector in the test volume of a line-source compact range. Vertical polarization at 10 GHz. (a) Center of range-reflector aperture. (b) 25.4 cm above center of range-reflector aperture.

are located near each other, one must be particularly careful to avoid standing waves between the antennas since this situation can cause measurement errors—especially in gain measurements. Such a situation usually is not a problem on an outdoor range because the receiving antenna intercepts only a small portion of the transmitted energy. This is analogous to reducing standing waves in a waveguide by inserting a pad attenuator between two discontinuities.

Interaction on a compact range can be controlled by configuring the feed and range geometry so that the test antenna intercepts only a small portion of the transmitted energy. Then the situation is similar to that encountered on an outdoor range, and interaction will not be a serious problem.

Stray Radiation Within Room: In effect, all of the aforementioned problem areas involve stray radiation—any radiation incident on the test antenna other than the desired collimated energy; however, they have dealt with stray radiation

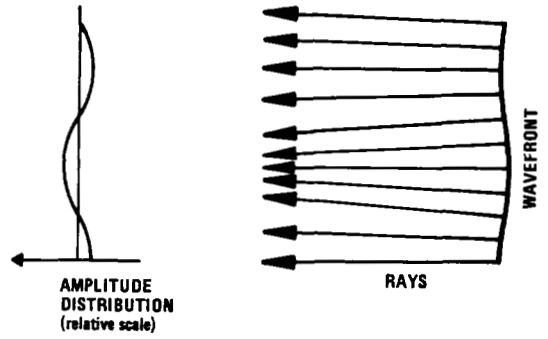

Fig. 24. Schematic representation of a uniform wavefront (incident from the right) which has small deviations from being planar. Since the rays are not collimated, the resulting amplitude distribution at some position to the left of the illustrated wavefront will be nonuniform.

generated by some component of the compact range itself. Another source of stray radiation is energy reflected or scattered by surrounding objects.

Such stray radiation can be reduced by placing absorbing material to intercept spillover radiation from the feed and by locating an absorbing panel behind the test antenna to catch the collimated beam. Other stray radiation, however, will be produced by means such as scattering from the test antenna and its positioner to other parts of the room and then back to the test antenna.

Past experience indicates that there was an ambient stray radiation level of about -50 to -60 dB relative to the collimated energy in the laboratory-type environments which were employed. To reduce the stray radiation below these levels, it may be necessary to isolate the ranges by surrounding them with absorbing material. The size of the enclosure and the amount of absorbing material required to isolate a compact range, however, would be much less than that required for conventional anechoic chambers which are designed to provide a $2D^2/\lambda$ range separation.

Surface Tolerances: One of the most critical factors in the design of a compact range is the matter of surface tolerances for the collimating reflector. Small deviations in the fabricated surface can cause undesirable effects in the field incident on the test antenna.

With a perfect collimating reflector, all reflected rays will be parallel and the field incident on the test antenna will have a plane front and a smooth amplitude distribution. Fabrication errors in the reflector, however, will cause a redistribution of directions in which the energy is radiated, and even relatively small errors will cause rays to deviate from paths parallel to the axis. This can result in significant variations in the amplitude distribution in the test region.

A simple schematic representation which illustrates the effects of small surface errors in the collimating reflector is shown in Fig. 24. If the wavefront incident from the right has small deviations from being planar, the rays will not be parallel, and this results in a nonuniform amplitude distribution at some position to the left of the illustrated wavefront. The calculation of field intensities in the test region of a compact range is more complex than indicated here, but Fig. 24 is useful to give one a simple intuitive feeling for problems that can be caused by small deviations in the range reflector.

A deviation of the range reflector can be described in simplified terms as having a shape, a maximum deviation (from the theoretical paraboloid), and a correlation area (size). For example, a deviation might be described as being spherical in

shape with a certain maximum deviation and with a certain diameter. A detailed analysis of the effects of fabrication errors in the range reflector of a compact range has not been made; however, we can draw some conclusions from intuitive reasoning and from approximations.

Suppose, for example, that a range reflector has small deviations which do not exceed about $\lambda/100$. Suppose, in addition, that the sizes of individual deviations are small—say, less than a square wavelength. The amplitude of the field at a point in the test region of the compact range will be the result of integrating contributions from all parts of the range reflector, and in this case the errors due to the deviations will tend to average out, leaving still a fairly uniform amplitude distribution across the test region. Suppose, on the other hand, that the sizes of the individual deviations are large—say, comparable to the area of the range reflector. In this case, the effect of the errors will be similar to that of a slightly defocused reflector, and the amplitude distribution will still be fairly uniform across the test region.

Deviations of intermediate sizes are more troublesome than either the small or large ones. The worst situation probably will be realized when the sizes of the deviations are comparable to a Fresnel zone [2, sec. 6.9.]. So in the fabrication of a range reflector, one must control not only the maximum deviations from the desired surface but also the areas over which the deviations are allowed to extend.

To better understand the effects of fabrication errors, Clayton [61] has approximated the change in amplitude at an observation point on the axis of a paraboloidal reflector due to a dimple centered on the axis and having a parabolic-shaped deviation error over one Fresnel zone. By integrating the contributions to the field over the dimple, he predicts that the fractional change in amplitude at the observation point will be $8\Delta/\lambda$, where Δ is the maximum deviation of the reflector and λ is the wavelength. This expression predicts a $\frac{1}{2}$-dB power change at the observation point for a maximum surface deviation of only 0.007λ.

The above approximation indicates that the range reflector must be fabricated with great care—particularly in the area in front of the test region, but the tolerance can be relaxed somewhat toward the edges of the range reflector. If the range reflector is constructed with sufficient accuracy, good results can be obtained with a compact range.

Applications

Compact ranges can be used for most applications in which the device under test must be illuminated by a uniform plane wave. Such applications include antenna pattern measurements, gain comparisons, boresight measurements [62], radar reflectivity measurements, and more recently, illumination of animals and humans to study biological effects of microwave radiation [63]–[65].

The chief advantage of compact ranges is the small size. In research and development activities, a compact range can be located in a laboratory near the design engineers. In manufacturing or rework facilities, a compact range can be located near the end of an assembly line. In both of these applications, the range can be located indoors where it will not be subject to adverse weather conditions. In addition, if testing must be performed in a bad electromagnetic environment, the compact range can be located in an absorber lined screen room free from outside interfering signals.

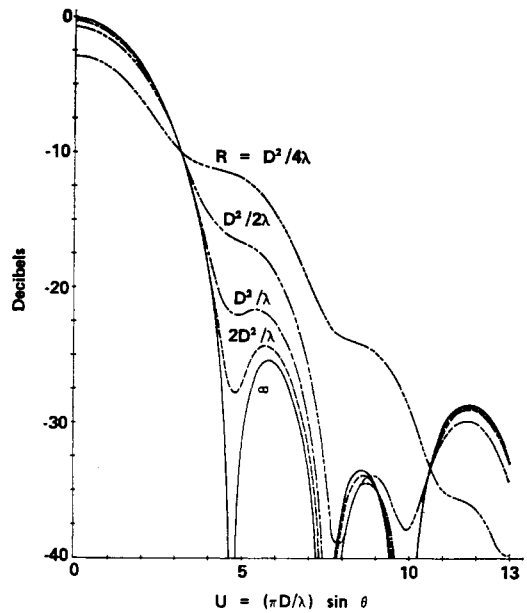

Fig. 25. Calculated infinite range patterns of a typical paraboloid focused at the indicated ranges.

Compact ranges are relatively new devices, and commercial models are just now being developed. It is felt that such ranges will prove very useful for many applications in the future.

Pattern Measurements with Antennas Focused at Less Than $2D^2/\lambda$

In the preceding sections two different methods were described for determining far-zone radiation patterns of narrow-beam antennas by measurements made in the regions of the apertures of the antennas. In this section the discussion will be directed toward making simulated far-field pattern measurements at test separations which are generally less than $2D^2/\lambda$, but removed from the region of the aperture itself. The measurements are made with the antenna under test focused to produce optimum radiation patterns at the test distance. The antenna is then refocused at infinity, and the patterns which are measured at the test distance are assumed to describe the far-field patterns of the refocused antenna within some range of error.

The need for refocusing after testing at short ranges is evident from Fig. 25, which presents calculated infinite range patterns of a typical paraboloidal antenna ($f/D=0.375$) which was focused at five test separations from $R=D^2/4\lambda$ to ∞. The aperture illumination was assumed to be circularly symmetric and of the form

$$f(r) = 0.316 + 0.684\cos^2(\pi r/2), \qquad 0.1 \le r \le 1$$
$$f(r) = 0, \qquad 0.1 > r > 1 \qquad (30)$$

where r is the normalized radius. This illumination represents a 10-dB edge taper with aperture blockage over the inner 10 percent of the radius. It will be observed that even at a test separation of $2D^2/\lambda$, there is significant sidelobe distortion, especially in the depth of the first null. In Fig. 26 measured patterns are presented of a 9.14-m diameter paraboloid ($f/D=0.41$) focused at $5D^2/6\lambda$ and then refocused at infinity to simulate the pattern distortion which would occur at in-

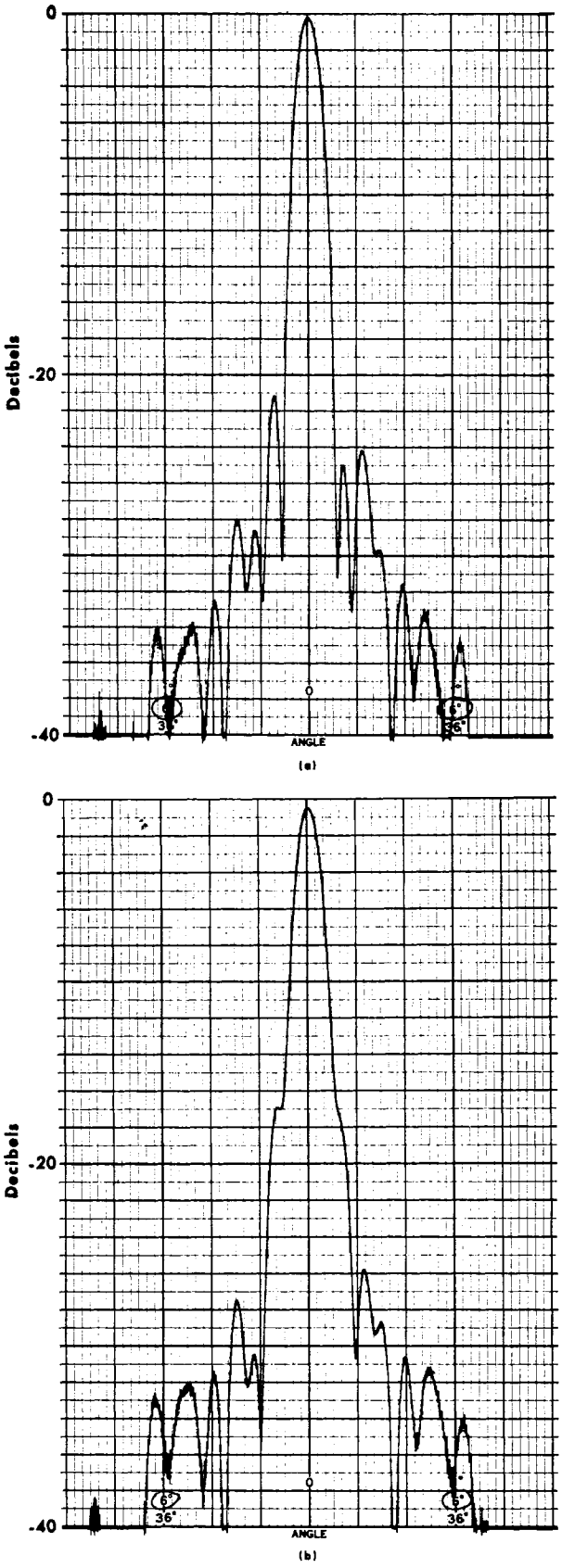

Fig. 26. Illustration of pattern distortion for typical paraboloid. (a) Focused at $5D^2/6\lambda$ and measured at the same range. (b) Focused at infinity and measured again at $5D^2/6\lambda$ to simulate operation at infinity after focusing at the shorter range.

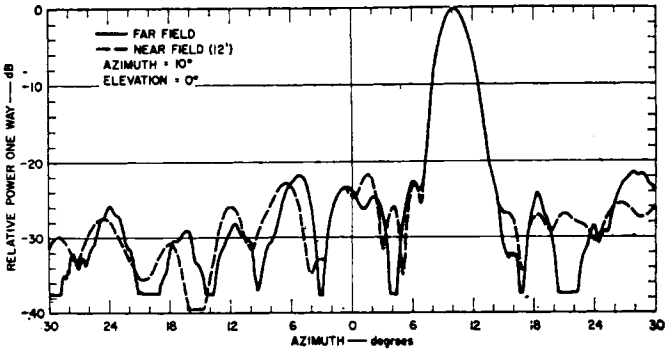

Fig. 27. Comparison of 3.65-m and far-field patterns of a 1.5×2.5-m planar array focused at 3.65 m and at infinity.

finite range without refocusing. It will be observed that there is a significant difference between the near-in sidelobes of the two patterns. It is also of interest to note that the farther-out sidelobes are relatively insensitive to the change in focal position of the feed. This is typical sidelobe behavior for small axial feed displacement. It is in keeping with predictions of aperture theory.

The technique of focusing at a short range applies to paraboloids or lenses which can be focused by axial positioning of the feed, linear arrays which can be physically bent along a circular arc of radius equal to the test distance [66], and to electronically phased arrays whose element phasing can be altered to provide focusing at the test distance [67], [68]. It also applies to antennas with parabolic-cylinder reflectors and line-source feeds [3, pp. 40–46] and to planar arrays which can be physically deformed to focus the array at the test distance. If focusing of an extended aperture is accomplished in only one plane, patterns can be made only in the plane of focus, and the gain of the antenna will be reduced from the far-field gain because of the aperture phase error in the orthogonal plane.

Ricardi reported on the near-field characteristics of a linear array [67] with references to the prior literature. Scharfman and August [68] investigated theoretically and experimentally the focusing properties of a planar phased array which could be focused electronically at distances as small as one aperture size. Fig. 27, from Scharfman and August [68], is a comparison of a far-field pattern with a near-field pattern of a *C*-band space-fed array of 1721 elements arranged in an ellipse approximately 2.5 by 1.5 m along the major and minor axes. The far-field pattern was made at a separation of 305 m ($\sim 8D^2/\lambda$), and the near-field pattern was made at a separation of 3.65 m; note that the patterns compare closely. Ricardi had previously shown that the gains for linear focused arrays were identical to the far-field gain for ranges as close as about one aperture length [67]. Scharfman and August reported agreement between gain measured at near-field ranges of 3.65 and 11 m with the far-field gain within a few tenths of a decibel.

The following discussions will be directed primarily toward focusing of paraboloids. Unlike electronically scanned arrays, which can be focused at short ranges without phase error except for digital roundoff error, paraboloids cannot be focused at close distances without introducing aberrations. In measurements of paraboloids at close distances the investigator is faced with at least the following questions: at how close a dis-

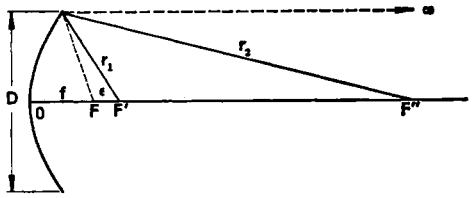

Fig. 28. Paraboloidal reflector focusing geometry.

tance measurements can be made without excessive error; what error is introduced by measuring at close distances; and what axial movement of the feed is required?

The problem of focusing paraboloids at small distances will be approached from the viewpoints of geometrical optics and physical optics. The geometrical optics approach was originally reported by Moseley [69] and by Cheng and Moseley [70]. They published an equation and curves for the required axial movement of the feed. We will examine the values of feed movement predicted by Cheng and Moseley. Then we will consider the degree of pattern distortion introduced by measurement at close distances, the minimum feasible separation between antenna under test and source antenna, and the effect of the source antenna.[4] Investigation of these effects requires application of physical optics; however, we will review the geometrical optics approach first.

Geometrical Optics Approach

The geometry relating to the focusing problems is given in Fig. 28. The reflector is assumed to be paraboloidal and the primary feed is initially assumed to be located with its phase center at F, the focal point of the paraboloid. It is assumed that the phase fronts of the wave emanating from the feed are spherical over the angular region subtended by the reflector so that a true phase center exists. Under these assumptions and assuming that geometrical optics applies, rays reflected from the paraboloid are parallel to the z axis, and the reflector is said to be focused at infinity. As the feed is moved axially away from the reflector through a distance ϵ to F', the reflected rays tend to focus at some point F'' on the z axis. Some aberration must now exist, however, since an *ellipsoidal* reflector would be required to produce aberration-free focusing at a finite range. For an ellipsoidal reflector with foci at F' and F'', all path lengths from F' to F'' via the reflecting surface would be identical. It therefore follows that a paraboloid, whose surface necessarily deviates from that of an ellipsoid, must exhibit some phase error over its aperture relative to the phase which would be exhibited by the ellipsoid.

For a given reflector diameter D the phase error increases as OF'' decreases, as the f/D ratio of the reflector decreases, and as the frequency increases. When the phase error caused by focusing becomes excessive, patterns measured at separations OF'' between the antenna under test at O and a source antenna located at F'' will differ significantly from the infinite range pattern which the antenna exhibits when the feed is at F. The magnitude of the residual phase error will be discussed later in this section.

[4] In this discussion the term "source antenna" will be used to describe the antenna at the opposite end of the antenna test range. For convenience, this term will be used whether the antenna under test transmits or receives, even though the "source antenna" is more properly called a "sampling" antenna in the former case.

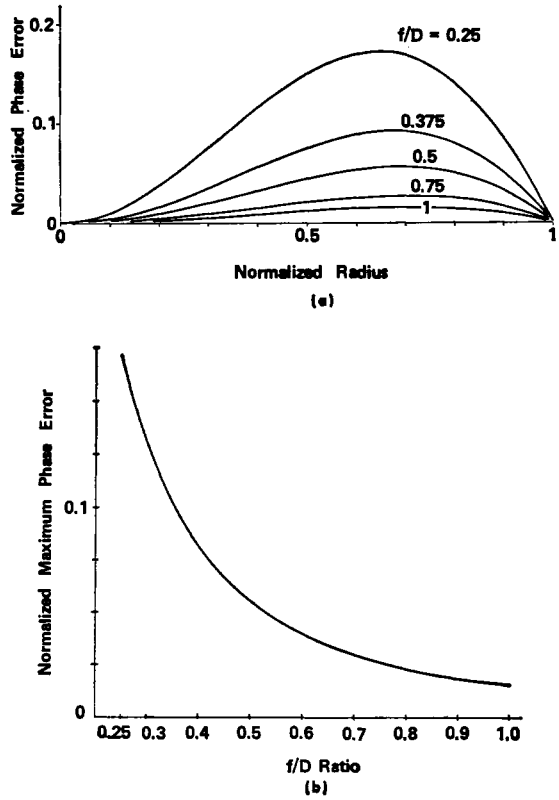

Fig. 29. Calculated residual phase error of paraboloids operated at focus distance. Unity phase error corresponds to $\pi D^2/4\lambda R$ radians. (a) Phase error as a function of radius. (b) Maximum phase error as a function of f/D ratio.

Cheng and Moseley proposed as a criterion for focusing the condition that

$$r_1 + r_2 = OF'' + OF + \epsilon \tag{31}$$

that is, that the path lengths from F' to F'' by reflection from the periphery of the reflector be identical with that by reflection from the apex They gave an approximation to the residual phase error for paraboloids focused under this criterion, which can be written

$$\Delta\phi = \frac{2\pi r^2}{\lambda}\left[\frac{D^2}{8R} - \frac{2\epsilon}{\left(\frac{4f}{D}\right)^2 + r^2}\right] \tag{32}$$

where r is radius in the aperture normalized to $D/2$.

Fig. 29 presents graphs of the calculated residual phase error of paraboloids focused under this criterion at finite separations R as a function of normalized radius. The f/D ratio of the paraboloid is the parameter. The phase error is normalized to the phase deviation between the fields at the periphery of the aperture and the center of the aperture with the separation between the source antenna and the antenna under test equal to R and the test antenna focused at infinity. These curves were made using geometrical optics to calculate the aperture field but without approximations in the focusing geometry [71]. They agree closely with the Cheng–Moseley approximation and apply with small error to ratios of R/D as small as 2 or 3.

Cheng and Moseley derived an approximate expression for

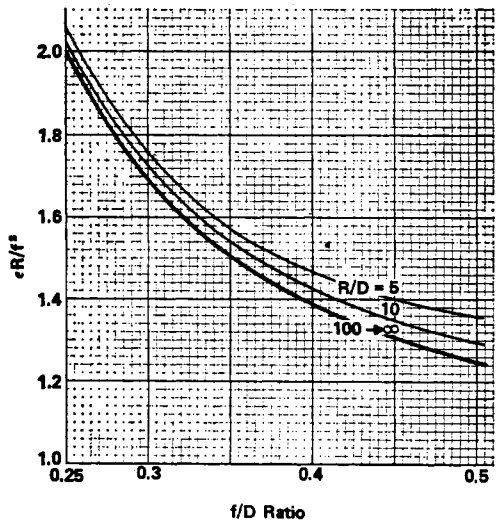

Fig. 30. Axial feed movement ϵ required to refocus paraboloid of focal length f and diameter D to infinity after focusing at test separation R. Curves are based on geometrical optics approach.

ϵ and published a set of graphs which relate ϵ to separation between the antenna under test and the source antenna [70] based on the approximation

$$\frac{\epsilon}{\lambda} = \frac{1}{n}\left[\left(\frac{f}{D}\right)^2 + \left(\frac{1}{4}\right)^2\right] \tag{33}$$

where $n = R\lambda/D^2$. The ratio ϵ/λ was presented as a function of n over the range of $R = 0.2D^2/\lambda$ to $50D^2/\lambda$, with the f/D ratio of the antenna under test as a parameter.

It should be noted that although Cheng and Moseley graphed ϵ/λ as an implicit function of λ through n, since ϵ is derived on the basis of geometrical optics, it is not a function of λ. This is reflected in the following expression from which (33) was derived.

$$\epsilon = \frac{1}{R}\left[f^2 + \left(\frac{D}{4}\right)^2\right]. \tag{34}$$

This equation is an approximation, but it has extremely small error and can be used for calculation of ϵ for almost all refocusing problems. It is instructive to compare (34) with an exact expression for ϵ using a digital computer to obtain an iterative solution [71]. For this purpose it is convenient to express (34) in the form

$$\frac{\epsilon R}{f^2} = 1 + \left(\frac{D}{4f}\right)^2. \tag{35}$$

The comparison is shown in Fig. 30. The heavy curve represents both the iterative solution for $R \geq 100$ and the solution to (35). It shows that the error in (34) or (35) vanishes as R/D approaches infinity. The error in the approximation is not of great importance when it represents a small phase error. For $R = D^2/2\lambda$ a 10-percent error in ϵ represents a 9° phase error. As one anticipates focusing at smaller multiples of D^2/λ, especially for antennas with larger f/D ratios, he must be more concerned about the error in refocusing.

Cheng in 1956 [72] and 1957 [73] reported additional investigations into the focusing of antennas for simulation of far-field radiation patterns in the near field. Cheng proposed three different methods for determining ϵ, and designated the three methods: the geometrical optics approach, the aperture phase approach, and the ellipsoidal reflector approach. He reported an inconsistency in the values of ϵ predicted by the three approaches. In 1971 Chu [74] commented on the inconsistency among the earlier results of Cheng. Chu showed that the inconsistency between the geometrical optics approach and the ellipsoidal reflector approach resulted because Cheng had matched the paraboloid with an "equivalent" ellipsoid only at the apex in the latter approach. He further pointed out that if the ellipsoidal and paraboloidal reflectors are made coincident at both the apex and the periphery, the ellipsoidal reflector approach reduces identically to the geometrical optics approach.

Physical Optics Approach

In the following paragraphs the value of ϵ, derived in the previous section using geometrical optics, will be related to its effect on the measured antenna pattern.

Cheng and Moseley [70] used minimum 3-dB beamwidth as a criterion of focus and found that the value of ϵ determined by this criterion for an assumed radial amplitude distribution of the form $F(r) = [1 - 2r/D)^2]^2$ was the same as that given by the geometrical optics approach. Calculations using the assumed aperture illumination of (30) made in connection with the present paper showed maximum gain for a value of ϵ which was 1 or 2 percent less than the value predicted by the geometrical optics approach.

Unfortunately, minimum beamwidth and maximum gain are both difficult to measure. In practice the criterion of focus probably used more than any other is the depth of the null between the first sidelobe and the main beam. We will employ this as the criterion of focus in the following discussion.

Although null depth is a sensitive indicator of focus, one has to recognize that the phasor addition of relatively small extraneous signals to the direct path signal can affect the accuracy of focusing regardless of the criterion employed. This is particularly true for antennas with a high percentage of aperture blockage. Multiple-bounce reflections between the feed-support structure and reflector can add to the radiated field to affect the gain, 3-dB beamwidth, sidelobe structure, and null positions. If such an antenna is focused at short range, the phase of the multiple-path energy will change compared with the phase when the feed is at the true focus, and can give a distorted presentation of the radiation characteristics. The following discussion relates to antennas in which such effects are minor. This includes a large fraction of antennas with gains above about 40 dB.

Calculations were made for the aperture illumination represented by (30) and for the same f/D ratio. Patterns were calculated by Fourier transformation of the aperture field for separations from $R = D^2/16\lambda$ to ∞ and for various values of axial feed position. The feed position is given by $k\epsilon$, where ϵ is the axial displacement predicted by the geometrical optics formulation represented by the curves of Fig. 30. The axial position is varied by letting k vary between zero and unity. In these calculations it was found that the deepest nulls occurred for values of k between 0.92 and 0.93 for all separations between $R = 2D^2/\lambda$ and $R = D^2/16\lambda$.

Fig. 31 shows calculated patterns for $R = D^2/8\lambda$. Maximum null depth was found to occur at a value of k near 0.925. The pattern for this value of k is compared with the pattern for

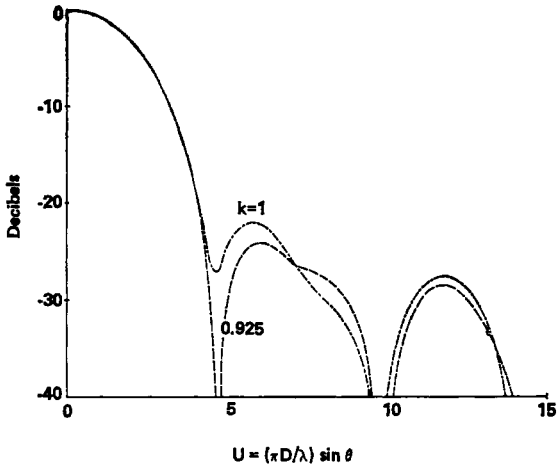

Fig. 31. Calculated principal-plane patterns of paraboloid operated at $D^2/8\lambda$ with feed position given by $k\epsilon$. Maximum null depth occurs for $k = 0.925$.

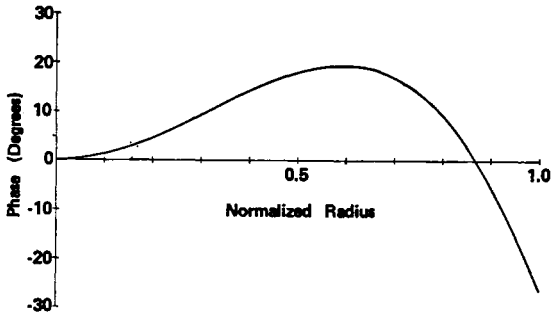

Fig. 32. Residual phase error of paraboloid focused at $D^2/8\lambda$ with feed position given by $0.925\ \epsilon$. See Fig. 33 for gain data.

$k = 1$. Fig. 32 is a graph of residual phase error as a function of radius for $k = 0.925$ for the f/D ratio of 0.375 employed in the calculations. Although these calculations were made with a theoretically perfect paraboloidal reflecting surface and with a specific aperture illumination, we believe that some value of k between 0.9 and 0.95 is a better value than unity for antennas with typical aperture illuminations.

Comments on Minimum Separation

Fig. 33 is a set of calculated patterns for an antenna under the previously assumed conditions, focused and tested from $R = 2D^2/\lambda$ down to $R = D/16\lambda$. The pattern at $R = 2D^2/\lambda$ is virtually identical with the infinite separation pattern. The sidelobes are seen to deviate significantly from those of the long-range patterns as the separation is decreased. Patterns were calculated for aperture diameters of 1000λ and 100λ so that the ratio of test separation to diameter changed from 62.5 to 6.25 at $R = D^2/16\lambda$. The patterns differed only slightly for the two cases. It is evident from Fig. 33 that, as the test range is decreased from $2D^2/\lambda$, there is a progressive deviation of the measured patterns from the pattern which would be obtained if the measurements were made at $2D^2/\lambda$ or greater.[5] Patterns calculated for an f/D ratio of 0.25 show similar character except that a given distortion occurs at slightly less than twice the separation that it occurs for a 0.375 f/D ratio.

[5] It is emphasized here that patterns measured at $R = 2D^2/\lambda$ will represent the infinite range pattern only after refocusing (see Fig. 25 for the deviation without refocusing).

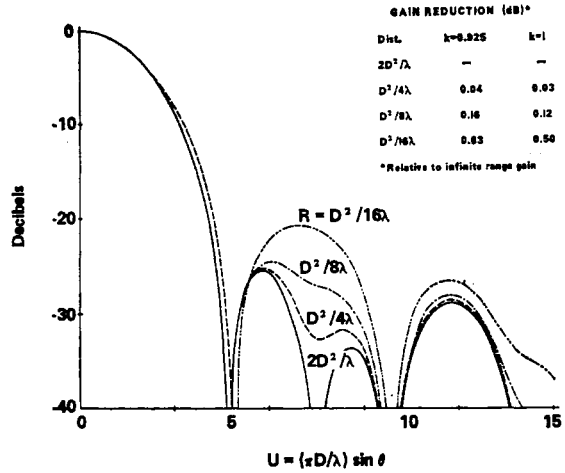

Fig. 33. Calculated principal-plane patterns of paraboloid focused at indicated test separations. The pattern for $2D^2/\lambda$ is virtually identical with the infinite separation pattern. The deepest nulls occur for k near 0.925. Note that gain is slightly higher for $k = 1$.

This result can be deduced from Fig. 29(b), which shows that the phase error for an f/D ratio of 0.25 at a given separation is almost twice that for the 0.375 ratio. These patterns are shown normalized to the same maximum gain level for ease of comparing sidelobe distortion. The gain degradation as a function of R is shown on the figure.

Fig. 34 presents a comparison of measured principal-plane patterns of a 1.83-m diameter paraboloid with an f/D ratio of 0.382, tested at a frequency of 7 GHz and focused at separations of $D^2/8\lambda$ and at $4D^2/\lambda$. The ratio of R/D at $D^2/8\lambda$ was 5.32 and the separation was 9.74 m. The calculated source antenna diameter for an aperture taper of $\frac{1}{4}$ dB at the reduced separation was 8.45 cm using the criterion developed in the next section. The actual source was a 3.2-cm by 4.3-cm waveguide horn. At the larger separation the source antenna was a 1.83-m diameter paraboloid.

In these measurements the general sidelobe character predicted in Fig. 33 can be observed. A crude attempt to refocus this antenna to the longer range of $4D^2/\lambda$ was made, and the resulting pattern is shown in Fig. 34(c). The calculated value of ϵ from Fig. 30, modified by the factor 0.925 and corrected to the larger separation of $4D^2/\lambda$ was 6.53 cm. The value of ϵ determined experimentally was 5.67 cm. The axial motion represented by the difference between the calculated and experimental values of ϵ represents a phase error of about 45°. This would correspond to the infinite-range phase error for an antenna which was focused at D^2/λ without refocusing. It is to be emphasized that this crude measurement serves only to illustrate the general validity of the method and problems encountered at small separations. Much additional work is required to permit quantitative assessment of the problems of focusing at ranges as small as $D^2/8\lambda$.

The pattern asymmetry in Fig. 34(c) results because the feed support did not provide for precise axial adjustment of the feed without lateral motion. The requirement for precise axial feed movement presents a problem if the antenna under test has pointing accuracy requirements, and this problem poses one of the major limitations in testing at small separations. When testing at separations of $D^2/2\lambda$ or greater, the main lobe is sufficiently well formed after refocusing to infinity that a check on the pointing angle can usually be made after refocusing. For extremely small ranges, broadening of

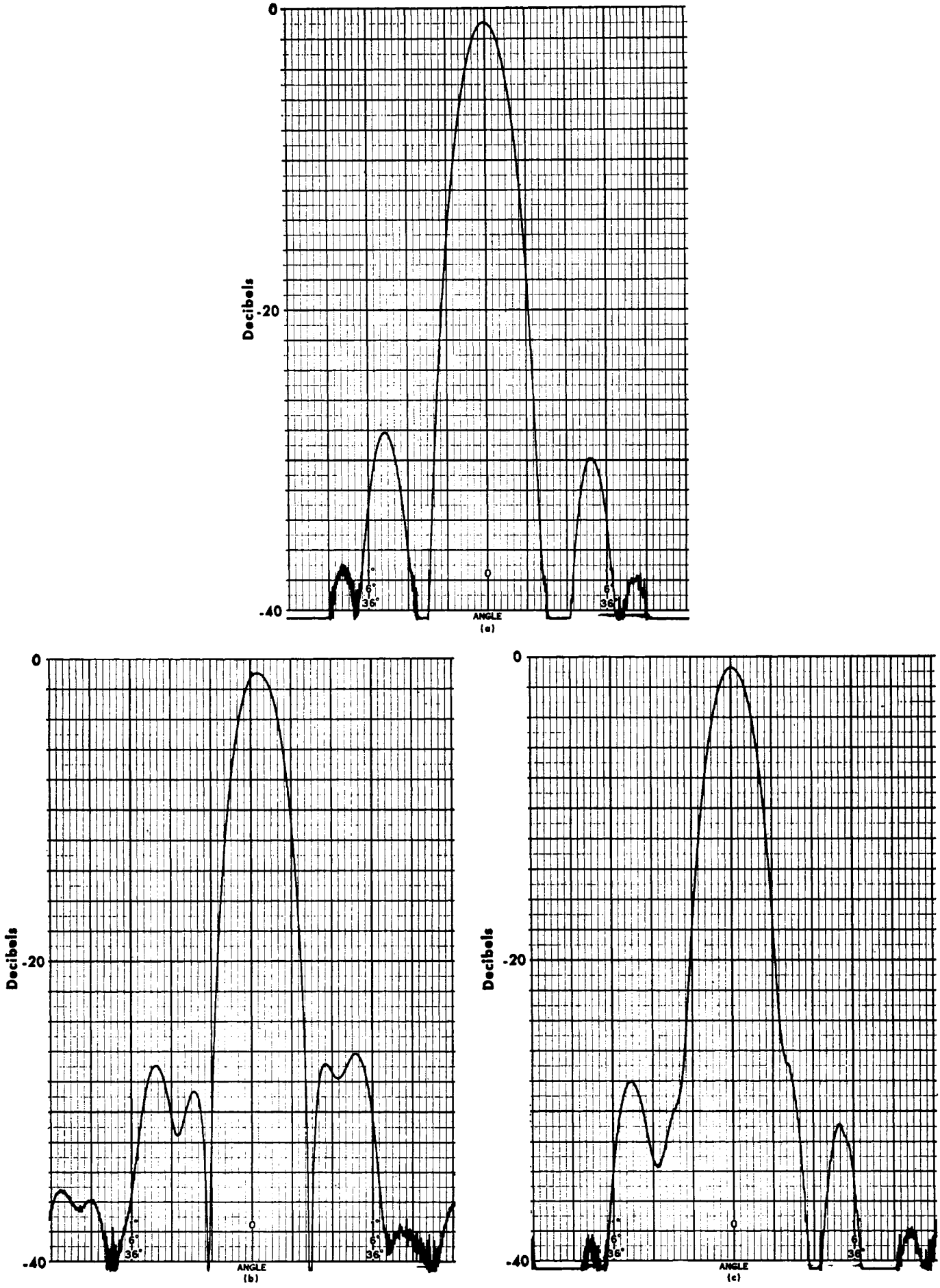

Fig. 34. Measured principal-plane patterns of 1.83-m diameter paraboloid with 0.382 f/D ratio at 7 GHz. (a) Focused and tested at $4D^2/\lambda$. (b) Focused and tested at $D^2/8\lambda$. (c) Tested at $4D^2/\lambda$ after refocusing from $D^2/8\lambda$ by movement of feed through calculated distance. Pattern asymmetry in (c) results because feed was not moved precisely in an axial direction.

the main lobe after refocusing (see Fig. 25) makes determination of the true pointing angle difficult. Monopulse and lobing antennas pose even more stringent problems than pencil-beam antennas because the angular accuracy requirements are usually much higher. Symmetry considerations show that antennas which exhibit perfect mirror symmetry about the boresight axis can be boresighted at close separations after refocusing to infinity, but analyses of individual problems are necessary for assessment of such errors where extreme precision is required.

An additional problem in testing at small separations is that the antenna under test is never identically paraboloidal, and often one of the purposes of pattern measurements is to evaluate the character of the reflector surface. If independent measurements are made which determine that the reflecting surface is paraboloidal within a negligible error, then focused measurements can be accomplished at quite small separations. If the character of the surface is unknown, a greater separation must be employed to insure a minimum performance in the radiating far field.

As an illustration of this point, suppose that an antenna is to be tested at a range of $D^2/8\lambda$. Let the surface actually be ellipsoidal when it is supposed to be paraboloidal and let the larger focal length, F'' in Fig. 28, of the ellipsoid be $D^2/8\lambda$. Patterns measured at this separation will appear to be well focused when the feed is at F' and, in fact, the patterns will be aberration-free. When the reflector is subsequently focused at infinity by moving the feed to F, the far-field patterns will contain significant distortion and increase in sidelobe levels from those expected.

One might counter that the aberration-free patterns measured at $D^2/8\lambda$ would lead to the conclusion that the reflector is ellipsoidal and would give a clue to the lack of validity of the measurement. Suppose, however, that the long focal length of the ellipsoid is $D^2/16\lambda$. The patterns measured at $D^2/8\lambda$ will now appear normally perturbed, but the far-field aberrations will be even more pronounced. Further, a distorted reflector is not likely to be ellipsoidal, but will likely have some shape which will produce an unidentifiable pattern distortion.

It is suggested that in general for antennas with f/D ratios of 0.35 or greater, unless extreme precision is required in measurements of pointing angle and maximum sidelobe levels, a separation as small as $D^2/2\lambda$ appears acceptable if some small departure from optimum gain after refocusing is allowable, even if the reflector surface characteristics are not known from other measurements. Quantitative determination of the gain reduction due to the residual phase error is beyond the scope of this paper. A minimum separation of $D^2/4\lambda$ appears practicable if documentation of sidelobe characteristics is not required. A separation of $D^2/8\lambda$ must be considered risky if good far-field focusing is required. For smaller f/D ratios the minimum range criteria should be increased to limit the residual aperture phase error to an equivalent value, as indicated in Fig. 29(b).

Effect of the Source Antenna

The values of ϵ calculated by Cheng and Moseley and by Chu are based on the assumption that the source antenna is a hypothetical point source. We will consider here the effect of a directive source antenna.

At first inspection it would appear that the value of ϵ for the case of a directive source antenna might be significantly different from that for the point source case. This is because of the nonzero aperture size of the source, requiring integrations over the apertures of both the antenna under test and the source, Fig. 35, to calculate the power transfer between the two antennas. Kay [53] and others have shown, however, from reciprocity considerations, that the effect of the integration over the source antenna can be represented with small error by an apparent modification of the amplitude and phase of the field which would exist on transmission over the aperture of the antenna under test. This approach simplifies the calculations and permits a direct assessment of the effect of the directivity of the source antenna on ϵ.

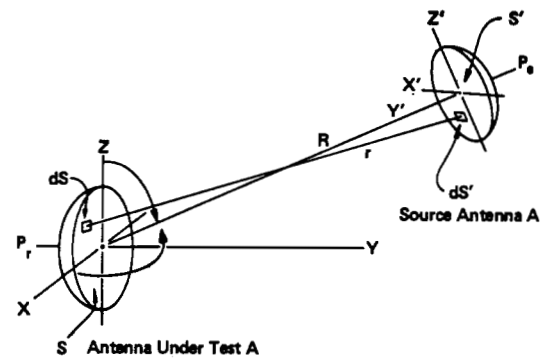

Fig. 35. Geometry illustrating integrations over source and test antennas required to calculate power transfer.

Let the antenna under test be focused at range R by adjusting for deepest nulls between the main lobe and first sidelobes. The value of ϵ through which the feed should be moved to achieve focus at infinity is that determined in the previous section.

Now let the radiation pattern be measured by a directive source antenna A', which produces a normalized field variation over the test aperture on the y axis when given by

$$\bar{g} = g(\xi, \eta)e^{j\gamma(\xi,\eta)} \tag{36}$$

where $g(0, 0) = 1$ and $\gamma(0, 0) = 0$. It can be shown that over the region of solid angle near the y axis, the radiation pattern of the antenna under test will be approximated closely by (13), but with its integrand multiplied by $\bar{g}$. If $\bar{g}$ is nearly equal to unity, then the patterns are virtually identical for a given axial position of the primary feed. Over angular regions farther removed from the axis the approximation is still closer than that represented by (36) because the projection of the aperture on the incoming wave is maximum when the direction of propagation from the source antenna is along the z axis, and hence $\bar{g}$ has maximum variation from unity.

It can be shown that, if the directivity of the source antenna is such that the field at the periphery of the test aperture varies less than $\frac{1}{4}$ dB from the field at the center, the amplitude function $g(\xi, \eta)$ in (36) is sufficiently near unity in this context. Calculated values of the phase deviation γ within the $\frac{1}{2}$-dB contour of a typical paraboloid as a function of the axial position of its feed are presented in Fig. 36. It can be seen that even for a grossly defocused source antenna the maximum value of γ is less than 3° even within the $\frac{1}{2}$-dB contour and is negligible within the $\frac{1}{4}$-dB contour. Thus $\bar{g}$ can be easily made to approach unity closely enough over the test aperture for the pattern measured with a directive source to be virtually identical with that measured using a hypothetical point source. Since the patterns are nearly identical, a single

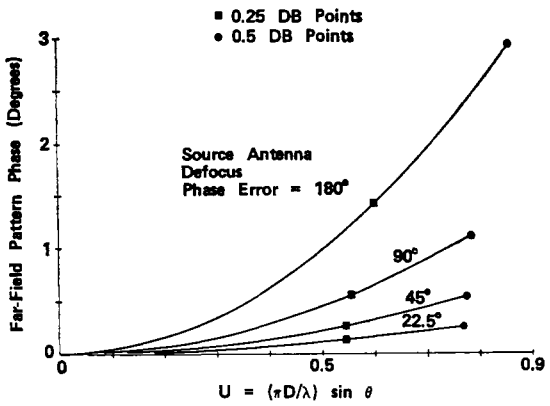

Fig. 36. Phase deviation from spherical phase front over test aperture caused by indicated defocusing of source antenna. The defocus phase error of the source antenna indicates the maximum deviation of the source-aperture phase front from planar.

value of feed movement ϵ applies to the two cases with negligible error.

As the test separation decreases it is necessary to decrease the directivity of the source antenna correspondingly to prevent the amplitude taper of the illumination over the test aperture from becoming excessive. It can be shown that the maximum diameter D_s of the source antenna for a $\frac{1}{4}$-dB taper over the test aperture can be approximated by

$$D_s = 0.37kD_t \tag{37}$$

where the test separation is kD^2/λ and D_t is the diameter of the test aperture [75].

Measurements of Dual-Reflector Antennas

Dual-reflector antennas can be broken into two classes, Cassegrain and shaped reflector. The Cassegrain antenna employs a concave paraboloidal main reflector and a convex hyperboloidal subreflector [76]. It is so named because it is derived from the Cassegrain telescope. The Gregorian antenna, derived from the Gregorian telescope, is similar to the Cassegrain type except that the subreflector is a concave ellipse. Since the basic equations for the Cassegrain also apply to the Gregorian, the latter is often considered a subclass of the former and the term "Cassegrain" is assumed to apply to both types. This will be done here.

Shaped dual-reflector antennas [77] are axially symmetric antennas which are similar to the Casegrain types except that the configurations of the reflector and subreflector are modified to provide a desired amplitude distribution while maintaining constant phase over the aperture of the secondary reflector, usually to increase the aperture efficiency.

It is well known that the performance of a Cassegrain antenna of a given focal length is determined by the performance of an equivalent paraboloid whose focal length is determined by mirroring the main reflector in the subreflector as seen from the feed [76]. This equivalence applies to the aperture distribution, coma, and cross-polarization characteristics. It also applies to the depth of focus, that is, the axial movement of the primary feed required to produce a given phase error. The equivalence applies, however, only to relatively small movements of the feed. Cassegrain antennas are usually designed to have long equivalent focal lengths, typically greater than 2. When such a Cassegrain antenna is to be focused at close range, the required axial feed movement usually becomes so large that the equivalent paraboloid concept does not apply. In addition, the illumination of the subreflector by the primary feed tends to be altered excessively. It is well known, however, that the focus is much more sensitive to axial movement of the subreflector than to movement of the primary feed [76]. These factors, in addition to the fact that it is usually difficult to move the primary feed, make it more practicable to accomplish focusing at short range by movement of only the subreflector. The subreflector is moved *toward* the main reflector to refocus to infinity.

It has been calculated by Cloete [78] that the required movement ϵ of the subreflector for a given main reflector f/D ratio and source separation R/D is within 3 percent of the value predicted for a prime focus reflector with the same f/D ratio. The calculated value of subreflector movement is essentially independent of the magnification. Hollis and Lyon [79] found that the residual aperture phase error due to focusing at a distance of $0.4D^2/\lambda$ was essentially the same as that indicated in Fig. 29(b) for a paraboloid having the f/D ratio of the main reflector. It should be emphasized that the f/D ratio in Fig. 29(b) is that of the main reflector, not the equivalent f/D ratio.

In the case of the typical Cassegrain antenna with a large depth of focus, if the phase center of the primary feed is known to reasonable accuracy, it can be located at the nominal focal point of the hyperboloid. The phase center of the primary feed must be known to an accuracy which is consistent with the depth of focus of the Cassegrain antenna. Fortunately, the depth of focus and the uncertainty in determining the axial position of the phase center increase together.

It is important that care be exercised to insure that only axial motion of the subreflector occurs since the beam direction and tilt are sensitive to lateral motion and angular misalignment of the subreflector. After the required refocusing has been accomplished, beam direction and pattern symmetry should be checked at the reduced range, as was discussed for prime-focus antennas.

Claydon [80] has investigated analytically the focusing characteristics of 3 shaped dual-reflector antennas, each with a main reflector diameter of 400 wavelengths. He defines *apparent focal length* as the distance from the vertex of the main reflector to the intersection of a line joining the extremities of the two reflectors with the axis of rotation. He presents curves of the aperture phase deviation as a function of aperture radius for three values of axial movement of the subreflector and the feed as parameters for an apparent f/D ratio of 0.31 and an apparent magnification of approximately 4.5.

One can conclude from the results of Claydon that, like the Cassegrain antenna, focusing a shaped dual-reflector antenna with large magnification is more practicable by displacement of the subreflector than by displacement of the primary feed. Analysis of the Claydon data shows that the required axial movement of the subreflector for an apparent f/D ratio of 0.31 and aperture diameter of 400λ for focusing at $R = 0.42D^2/\lambda$ was 0.35λ; see Fig. 37. This compares with 0.38λ for a prime focus antenna of the same focal length. The maximum value of the residual aperture phase error due to focusing at this distance is essentially that indicated in Fig. 29(b) for a paraboloid with focal length equal to the apparent focal length as defined by Claydon. The phase error as a function of radius appears to have similar character to that of Fig. 29(a), but with a slightly different distribution near the center of the aperture.

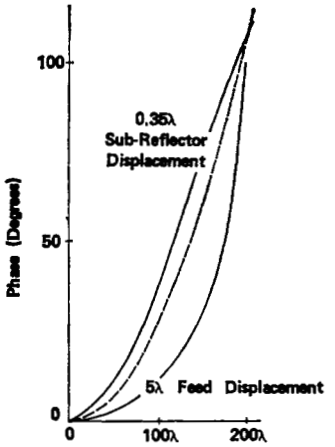

Fig. 37. Calculated aperture phase error for a shaped dual-reflector antenna 1) by movement of the subreflector axially through 0.35 λ, and 2) by movement of the feed axially through 5λ. The aperture quadratic phase error due to the testing at $0.42D^2/\lambda$ is shown by the dashed curve. (From Claydon, [80].)

The Claydon data further indicate that the residual aperture phase error for a feed-horn displacement which would focus the shaped dual-reflector antenna at $0.42D^2/\lambda$ was greater by a factor of about 2 than that for the subreflector movement which would cause focusing at the same range. The feed-horn displacement for focusing at this range employing the criterion of equal phases at the center and periphery of the aperture was approximately 5λ. This is the same as that predicted by (33).

Concluding Remarks

The body of this paper has been concerned primarily with three fundamentally different techniques for determining antenna far-field patterns from measurements made within the radiating near-field region. Each technique has individual advantages and limitations, and these features determine whether a technique is suitable for a particular application. However, when properly employed, each technique can be used with confidence to determine far-field patterns without requiring far-field separations between test and measurement antennas.

The first technique, in which the field near the antenna aperture is sampled with a scanning probe, requires an accurate probe positioner to permit sampling of the near field at known positions. The near-field data must be stored, and a digital computer is needed to transform the near-field data into far-field patterns. Although very accurate near-field measurements are required, a *complete* radiation pattern over a solid angle can be calculated—not merely a few cuts through the pattern. This is a very valuable feature, for example, when one must be assured that no extraneous sidelobes above a certain level exist within a certain solid angle. An enormous amount of measurement time on a far-field range could be required to make a similar solid-angle pattern using conventional techniques. Another important advantage of this near-field technique is that the field probe can be taken to the test antenna in some cases when the antenna cannot be removed from its operating environment.

The second technique, in which an incident plane wave is created near the test antenna by a compact range, requires an accurate range reflector and feed. Otherwise, the instrumentation is similar to that of a conventional far-field range. The useful frequency range of a compact range is limited on the upper end by fabrication errors of the range reflector and on the lower end by diffraction effects of the reflector edges and by direct radiation from the feed. At lower frequencies, it is more difficult to use absorbing material to reduce direct radiation from the range feed to the test antenna. The chief advantage of a compact range is its small size which allows it to be located indoors; the small size also reduces the requirements for microwave absorbing material. A chief limitation is that the range reflector must be larger than the antenna under test; in addition, the reflector must be constructed very accurately. Compact ranges are very versatile, however, since they can be used for antenna pattern measurements, gain comparisons, boresight measurements, radar reflectivity measurements, and many other applications which require the creation of an incident plane wave at microwave frequencies.

The third technique, in which the test antenna is focused within the radiating near field for pattern measurements, is quite simple to employ; however, it is applicable only to antennas which can be focused for testing and then refocused to infinity for operation. The chief advantage of this technique is that pattern measurements can be made in the radiating near field for many antennas when available ranges are not long enough for far-field measurements.

The third technique (focusing) usually is employed only when a far-field range of sufficient length is not available; however, it is important to note that the first two techniques (field probing and compact range) usually are employed because they have certain advantages over conventional outdoor ranges. The techniques, field probing and compact range, have not been employed extensively yet because they were developed only recently, but it is anticipated that both techniques will be employed more in the future as they become better known and as commercial models become more readily available.

References

[1] D. T. Paris and F. K. Hurd, *Basic Electromagnetic Theory*. New York: McGraw-Hill, 1969, sec. 10.15.
[2] R. C. Hansen *et al.*, "IEEE test procedure for antennas; Number 149 (Revision of 48 IRE 252) January 1965," *IEEE Trans. Antennas Propagat.*, vol. AP-13, pp. 437–466, May 1965.
[3] R. C. Hansen, "Aperture theory," in *Microwave Scanning Antennas*, R. C. Hansen, Ed. New York: Academic Press, 1964, pp. 31–32.
[4] S. Silver, *Microwave Antenna Theory and Design* (Radiation Lab. Ser.), vol. 12. New York: McGraw-Hill, 1949, sec. 6.9.
[5] J. P. Shanklin, "Pattern measurements of large fixed antennas," *IRE Trans. Instrum.*, vol. I-4, pp. 16–22, Oct. 1955.
[6] H. Brueckmann, "Antenna pattern measurement by satellite," *IEEE Trans. Antennas Propagat.*, vol. AP-11, pp. 143–147, Mar. 1963.
[7] J. T. Kennedy and J. W. Rosson, "The use of solar radio emission for the measurement of radar angle errors," *Bell Syst. Tech. J.*, pp. 1799–1812, Nov. 1962.
[8] J. A. Stratton, *Electromagnetic Theory*. New York: McGraw-Hill, 1941, ch. 8.
[9] J. D. Dyson, "Antenna near field measurements," in *Electromagnetics and Antennas* (a series of lectures from the University of Illinois College of Engineering), pp. 57–114, 1967.
[10] H. E. Gihring and G. H. Brown, "General consideration of tower antennas for broadcast use," *Proc. IRE*, vol. 23, pp. 311–356, Apr. 1935.
[11] B. C. Dunn, Jr., and R. W. P. King, "Microwave field measurements, I, Measurement of surface-current and charge distributions on metal surfaces at microwave frequencies," Cruft Lab., Harvard University, Tech. Rep. 71, Sept. 1, 1949, DDC ATI-66029.
[12] S. A. Schelkunoff, *Electromagnetic Waves*. New York: Van Nostrand, 1943, ch. 6.
[13] J. H. Richmond and T. E. Tice, "Probes for microwave near-field

measurements," *IRE Trans. Microwave Theory Tech.*, vol. MTT-3, pp. 32–34, Apr. 1955.
[14] G. A. Woonton, "The probe antenna and the diffraction field," The Eaton Electron. Res. Lab., McGill Univ., Montreal, Canada, Tech. Rep. 17, July 1952.
[15] R. B. Borts and G. A. Woonton, "The effect of the directivity of the probe upon the measurement of aperture fields," The Eaton Electron. Res. Lab., McGill Univ., Montreal, Canada, Tech. Rep. 21, July 1952.
[16] C. L. Andrews, "Microwave probes for electric fields near metal surfaces," *IEEE Trans. Antennas Propagat.*, vol. AP-16, pp. 441–445, July 1968.
[17] R. Plonsey, "Surface current measurements with an electric probe," *IRE Trans. Microwave Theory Tech.*, vol. MTT-10, pp. 214–217, May 1962.
[18] H. Whiteside and R. W. P. King, "The loop antenna as a probe," *IEEE Trans. Antennas Propagat.*, vol. AP-12, pp. 291–297, May 1964.
[19] R. Justice and V. H. Rumsey, "Measurement of electric field distributions," *IRE Trans. Antennas Propagat.*, vol. AP-3, pp. 177–180, Oct. 1955.
[20] A. L. Cullen and J. C. Parr, "A new perturbation method for measuring microwave fields in free space," *Proc. Inst. Elec. Eng.*, vol. 102B, pp. 836–844, Nov. 1955.
[21] J. H. Richmond, "A modulated scattering technique for measurement of field distributions," *IRE Trans. Microwave Theory Tech.*, vol. MTT-3, pp. 13–15, July 1955.
[22] M. K. Hu, "Study of near-zone fields of large aperture antennas," Syracuse Univ. Res. Inst., Electrical Engineering Dep., Syracuse, N. Y., Rep. EE282-574F1, pt. 1 of two, Apr. 1957.
[23] R. F. Harrington, "Small resonant scatterers and their use for field measurements," *IRE Trans. Microwave Theory Tech.*, vol. MTT-10, pp. 165–174, May 1962.
[24] C. H. Walter, *Traveling Wave Antennas*. New York: McGraw-Hill, 1965, ch. 2.
[25] T. T. Taylor, "Design of line-source antennas for narrow beamwidth and low side lobes," *IRE Trans. Antennas Propagat.*, vol. AP-3, pp. 16–28, Jan. 1955.
[26] H. A. Ecker, "Study of directivity optimization for linear antennas," Antenna Lab., Dep. Electrical Engineering, The Ohio State Univ. Res. Foundation, Tech. Rep. AFAL-TR-66-38, Feb. 28, 1966.
[27] N. J. Gamara, "Pattern predictability on the basis of aperture phase and amplitude distribution measurements," Electronic Defense Lab., Mountain View, Calif., Tech. Memo. EDL-M247, ASTIA Doc. AD 236 298, Mar. 25, 1960.
[28] R. M. Goodman, Jr., R. C. Johnson, H. A. Ecker, and W. K. Rivers, Jr., "A folded geodesic Luneberg lens antenna," in *Proc. 17th Annu. Symp. on USAF Antenna Research and Development*, Univ. of Illinois, Nov. 1967.
[29] M. Born and E. Wolf, *Principles of Optics*, 2nd ed. Oxford, England: Pergamon, 1964, ch. 8.
[30] D. T. Paris, "Digital computer analysis of aperture antennas," *IEEE Trans. Antennas Propagat.* (Commun.), vol. AP-16, pp. 262–264, Mar. 1968.
[31] L. Clayton, Jr., J. S. Hollis, and H. H. Teegardin, "A wide frequency range microwave phase-amplitude measuring system," in *Abstracts of the 11th Annu. USAF Symp. on Antenna Research and Development*, Univ. of Illinois, Oct. 1961.
[32] L. Clayton, Jr., and J. S. Hollis, "Calculation of microwave antenna radiation systems, by the Fourier integral method," *Microwave J.*, vol. 3, pp. 59–66, Sept. 1960.
[33] H. G. Booker and P. C. Clemmow, "The concept of an angular spectrum of plane waves, and its relation to that of polar diagram and aperture distribution," *Proc. Inst. Elec. Eng.*, vol. 97, pt. III, pp. 11–17, Jan. 1950.
[34] D. M. Kerns, "Correction of near-field antenna measurements made with an arbitrary but known measuring antenna," *Electron. Lett.*, vol. 6, pp. 346–347, May 28, 1970.
[35] D. M. Kerns and E. S. Dayhoff, "Theory of diffraction in microwave interferometry," *J. Res. Nat. Bur. Stand.*, vol. 64B, pp. 1–13, Jan.–Mar. 1960.
[36] E. B. Joy and D. T. Paris, "Spatial sampling and filtering in near-field measurements," *IEEE Trans. Antennas Propagat.*, vol. AP-20, pp. 253–261, May 1972.
[37] J. Brown, "A theoretical analysis of some errors in aerial measurements," IEEE Monograph No. 285 R, pp. 343–351, Feb. 1958.
[38] J. Brown and E. V. Jull, "The prediction of aerial radiation patterns from near-field measurements," Inst. Elec. Eng. (London), Paper 3649 E, pp. 635–644, Nov. 1961.
[39] E. V. Jull, "An investigation of near-field radiation patterns measured with large antennas," *IRE Trans. Antennas Propagat.*, vol. AP-10, pp. 363–369, July 1962.
[40] ——, "The estimation of aerial radiation patterns from limited near-field measurements," *Proc. Inst. Elec. Eng.*, vol. 110, pp. 501–506, Mar. 1963.
[41] W. M. Leach, Jr., "Probe compensated near-field measurements on a cylinder," Ph.D. dissertation, Georgia Inst. Technol., Aug. 1972.
[42] F. Jensen, "Electromagnetic near-field far-field correlations," Ph.D. dissertation, Tech. Univ. of Denmark, Lyngby, July 1970.
[43] A. C. Ludwig, "Near-field far-field transformations using spherical-wave expansions," *IEEE Trans. Antennas Propagat.*, vol. AP-19, pp. 214–220, Mar. 1971.
[44] J. R. James and L. W. Longdon, "Perdiction of arbitrary electromagnetic fields from measured data," *Alta Freq.*, vol. 38, pp. 286–290, May 1969.
[45] P. C. Clemmow, *The Plane Wave Spectrum Representation of Electromagnetic Fields*. London, England: Pergamon, 1966.
[46] R. C. Baird, A. C. Newell, P. F. Wacker, and D. M. Kerns, "Recent experimental results in near-field antenna measurements," *Electron. Lett.*, vol. 6, pp. 349–351, May 28, 1970.
[47] P. D. Potter, "Application of spherical wave theory to Cassegrainian-fed paraboloids," *IEEE Trans. Antennas Propagat.*, vol. AP-15, pp. 727–736, Nov. 1967.
[48] G. A. Woonton, R. B. Borts, and J. A. Carruthers, "Indoor measurement of microwave antenna radiation patterns by means of a metal lens," *J. Appl. Phys.*, vol. 21, pp. 428–430, May 1950.
[49] G. A. Woonton, J. A. Carruthers, H. A. Elliott, and E. C. Rigby, "Diffraction errors in an optical measurement at radio wavelengths," *J. Appl. Phys.*, vol. 22, pp. 390–396, Apr. 1951.
[50] M. H. Chapman, M.Sc. thesis, McGill Univ., Montreal, Canada, 1951; also G. Bekefi, "Studies in microwave optics," McGill Univ., Tech. Rep. 38, ASTIA Doc. DDC AD110152, under Contract AF 19(221)-81, p. 219, Mar. 1957.
[51] J. R. Mentzer, "The use of dielectric lenses in reflection measurements," *Proc. IRE*, vol. 41, pp. 252–256, Feb. 1953.
[52] J. H. Crysdale, M.Sc. thesis, McGill Univ., Montreal, Canada, 1953.
[53] A. F. Kay, "Far field data at close distances," Tech. Res. Group, New York, N. Y., Final Rep. sec. 2, ASTIA Doc. DDC AD53507, under Contract AF 19(604)-1126, Oct. 1954.
[54] R. C. Johnson, "Antenna range for providing a plane wave for antenna measurements," U.S. Patent 3 302 205, Jan. 31, 1967.
[55] R. C. Johnson and R. J. Poinsett, "Compact antenna range techniques," Rome Air Devel. Cen., Griffiss AFB, Rome, N. Y., under Contract AF 30(602)-3594, Final Rep. RADC-TR-66-15, Apr. 1966.
[56] R. C. Johnson and A. L. Holliman, "Improved point-source and line-source compact antenna ranges," Rome Air Devel. Cen., Griffiss AFB, Rome, N. Y., under Contract AF 30(502)-4269, Tech. Rep. RADC-TR-67-463, Oct. 1967.
[57] H. A. Ecker and R. A. Moore, "Compact radar reflectivity ranges," Rome Air Devel. Cen., Griffiss AFB, Rome, N. Y., under Contract AF 30(602)-4269, Tech. Rep. RADC-TR-68-204, July 1968.
[58] R. C. Johnson, H. A. Ecker, and R. A. Moore, "Compact range techniques and measurements," *IEEE Trans. Antennas Propagat.*, vol. AP-17, pp. 568–576, Sept. 1969.
59] A. B. Pippard, "The hoghorn—An electromagnetic horn radiator of medium-sized aperture," *J. Inst. Elec. Eng.*, pt. IIIA, vol. 93, pp. 1536–1538, Oct. 1946.
60] C. E. Ryan, Engineering Experiment Station, Georgia Institute of Technology, Atlanta, Ga. 30332; private communications.
[61] L. Clayton, Scientific-Atlanta, Inc., Atlanta, Ga. 30324; private communications.
[62] T. G. Hickman and R. C. Johnson, "Boresight measurements utilizing a compact range," in *Abstracts 1972 Spring USNC/URSI Meet.* (Washington, D. C., Apr. 13–15, 1972), p. 11.
[63] H. L. Bassett, H. A. Ecker, R. C. Johnson, and A. P. Sheppard, "New techniques for implementing microwave biological-exposure systems," *IEEE Trans. Microwave Theory Tech.*, vol. MTT-19, pp. 197–205, Feb. 1971.
[64] F. L. Cain and H. A. Ecker, "Illumination equipment for electromagnetic radiation hazard research," Eng. Experiment Sta., Georgia Inst. Technol., Atlanta, Ga. 30332, Final Eng. Rep. under Contract N00014-67-A-0159-0008, Oct. 1971.
[65] R. T. Davis, "Long range radiation hazard experiment gets underway using human volunteers," *Microwaves*, vol. 11, pp. 12–14, Apr. 1972.
[66] M. D. Fahey, T. C. Pierce, and W. G. Spaulding, "Focused phased array measurements," *IEEE Trans. Antennas Propagat.* (Commun.), vol. AP-21, pp. 564–565, July 1973.
[67] L. J. Ricardi, "Near-field characteristics of a linear array," in *Electromagnetic Theory and Antennas*, E. C. Jordan, Ed. New York: Pergamon, 1963, pp. 1301–1305.
[68] W. E. Scharfman and G. August, "Focused antenna pattern techniques for phased array radar," Stanford Res. Inst., Final Rep., Project 7528, June 1970.
[69] S. T. Moseley, "On-axis defocus characteristics of the paraboloidal reflector," Elec. Eng. Dep., Syracuse Univ. Final Rep., USAF Contract AF30(602)-925, Aug. 1, 1954.
[70] D. K. Cheng and S. T. Moseley, "On-axis defocus characteristics of the paraboloidal reflector," *IRE Trans. Antennas Propagat.*, vol. AP-3, pp. 214–216, Oct. 1955.

[71] J. Cloete and J. S. Hollis, unpublished notes, Scientific-Atlanta, Inc., Atlanta, Ga., 1972.
[72] D. K. Cheng, "Microwave aerial testing at reduced ranges," *Wireless Eng.*, pp. 234–237, Oct. 1956.
[73] ——, "On the simulation of Fraunhofer radiation patterns in the Fresnel region," *IRE Trans. Antennas Propagat.*, vol. AP-5, pp. 399–402, Oct. 1957.
[74] T. S. Chu, "A note on simulating Fraunhofer radiation patterns in the Fresnel region," *IEEE Trans. Antennas Propagat.* (Commun.), vol. AP-19, pp. 691–692, Sept., 1971.
[75] J. S. Hollis *et al.*, "Microwave antenna measurements," Scientific-Atlanta, Inc., Tech. Rep., pp. 14–27, 1970.
[76] P. W. Hannan, "Microwave antennas derived from the Cassegrain telescope," *IRE Trans. Antennas Propagat.*, vol. AP-9, pp. 140–153, Mar. 1961.
[77] V. Galindo, "Design of dual-reflector antennas with arbitrary phase and amplitude distributions," *IEEE Trans. Antennas Propagat.*, vol. AP-12, pp. 403–408, July 1964.
[78] J. Cloete, CSIR Praetoria, Republic of South Africa, unpublished notes, Scientific-Atlanta, Inc., Atlanta, Ga., 1972.
[79] T. J. Lyon and J. S. Hollis, Scientific-Atlanta, Inc., Atlanta, Ga., 1969.
[80] B. Claydon, "The effects of phase errors caused by axial displacement of the feedhorn on subreflector in a shaped dual reflector system," *IEE Conf. on Earth Station Technology* (Oct. 14–16, 1970), pp. 162–168.

Phenomenological and Electron-Theoretical Study of the Electrodynamics of Rotating Systems

TOSHIYUKI SHIOZAWA

Abstract—**A phenomenological and electron-theoretical study of the electrodynamics of rotating systems is developed in the three-dimensional form. In the former part of the present paper, the electromagnetic field equations in an isotropic and homogeneous medium performing arbitrary accelerated motion relative to an inertial reference frame are derived from the phenomenological viewpoint, under the assumptions that the observer is at rest in the inertial or rotating reference frame and that the macroscopic properties of the material medium are not changed by the acceleration acting upon it. With the aid of the classical electron theory, the latter part of the present paper discusses the electromagnetic field equations in rotating media as viewed from the inertial or rotating frame, presenting an electron-theoretical basis for the electrodynamics of rotating media. In addition, the electromagnetic effects caused by the inertial forces accompanying the rotational motion, i.e., the centrifugal and Coriolis forces, are investigated in detail.**

I. Introduction

THE ELECTRODYNAMICS of moving media was founded in 1908 by Minkowski [1], on the basis of the special theory of relativity. Although new formulations [4]–[6] to replace Minkowski's theory [2], [3] have been presented by several authors after its appearance, it has been recently clarified by Tai [7] that they are not independent of the Minkowski formulation but rather can be deduced directly from it by the appropriate linear transformations.[1] Thus we may now consider Minkowski's theory as giving the basis for the macroscopic electromagnetism. However, Minkowski's theory seems to be unsatisfactory in that it can be applied only to the electromagnetic phenomena in inertial reference frames: it is applicable only to the case where both observers and material media are at rest in inertial frames. Most recently, several attempts [9]–[12] have been made to extend Minkowski's theory to the case that observers or material media are performing accelerated motion with respect to inertial frames. In these attempts, the electromagnetic field equations in accelerated systems have been obtained from those in inertial reference frames by means of the mathematical tool in the general theory of relativity, i.e., the tensor calculus in the four-dimensional Riemannian space [2], [13]–[15]. Although the tensor calculus is an elegant and useful means for describing the physical phenomena in accelerated systems, it is also possible, as in the case of the Maxwell–Minkowski equations in inertial frames [16], [22], to develop the electrodynamics of accelerated systems in the three-dimensional form, without using the tensor calculus. The purpose of this paper is to derive, by the latter method, the electromagnetic field equations for the typical cases of accelerated motion that observers or material media are uniformly rotating with respect to inertial reference frames.

In this article, let us discuss the aforementioned problem from two distinct points of view, namely, from the phenomenological and electron-theoretical viewpoints. By the phenomenological viewpoint is meant a viewpoint in which one describes the electromagnetic effects of matter in terms of given parameters such as permittivity ϵ, permeability μ, and conductivity σ, without inquiring into its internal structures. In this sense, the works presented so far [9]–[12] stand all on the phenomenological viewpoint. In the electron-theoretical point of view, on the other hand, material media are regarded as consisting of positively charged nuclei and negatively charged electrons, and their electromagnetic effects are taken into account by considering the interaction of electromagnetic fields with the aggregate of these charged particles. For the case of material media performing accelerated motion, in

Manuscript received May 7, 1973; revised August 6, 1973.
The author is with the Department of Electrical Communication Engineering, Osaka University, Suita, Osaka 565, Japan.

[1] Recently, a comparative study of various formulations of electrodynamics of moving media has also been presented by Penfield and Haus [8], but they have not discussed the constitutive relations between field vectors. As pointed out by Tai [7], the constitutive relations play an important role in the electrodynamics of moving media.

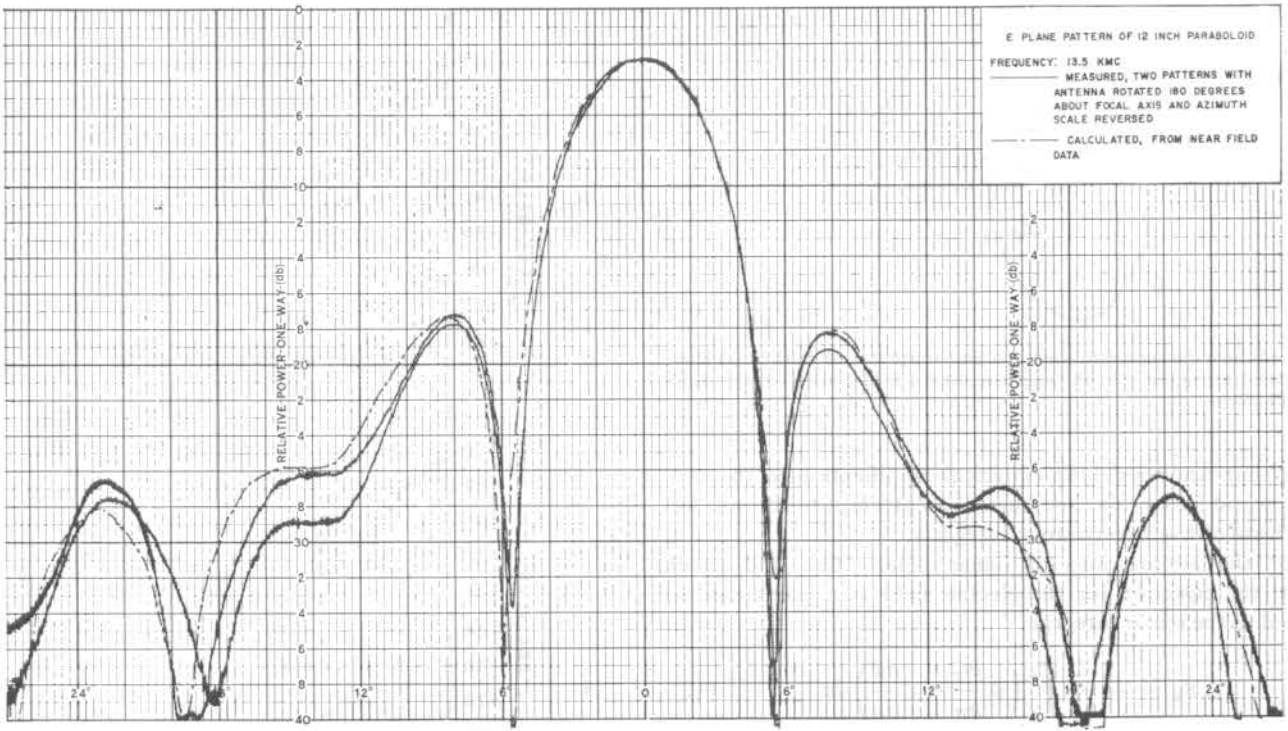

Fig. 7. Measured and computed E-plane patterns of a 30.5-cm paraboloidal antenna operating at 13.5 GHz. Two measured patterns are shown with the antenna rotated 180° about its focal axis between the two measurements.

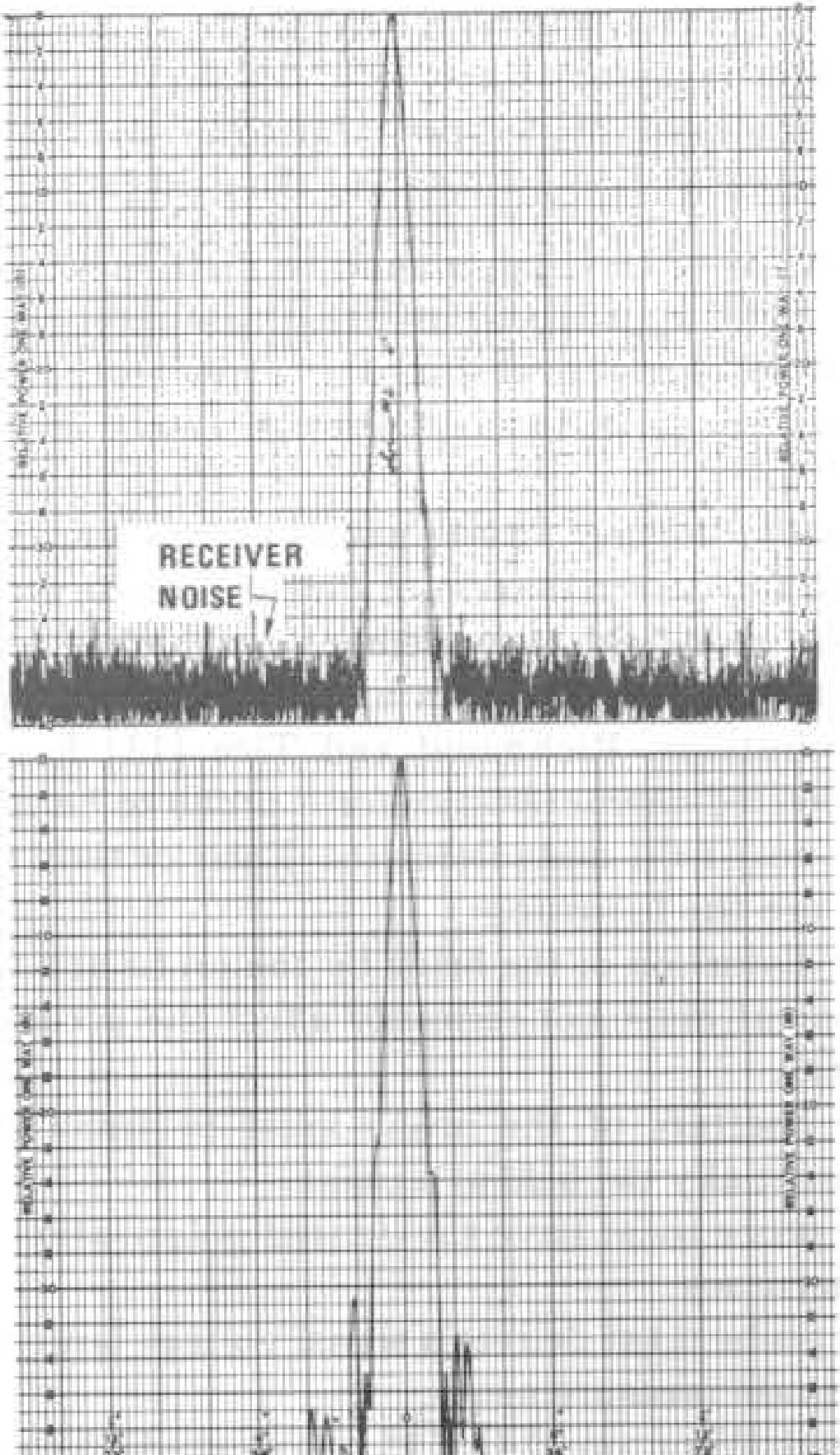

Fig. 4. Measured and computed far-field (H-plane) antenna patterns for a folded geodesic Luneberg lens antenna operating at 4.3 mm.

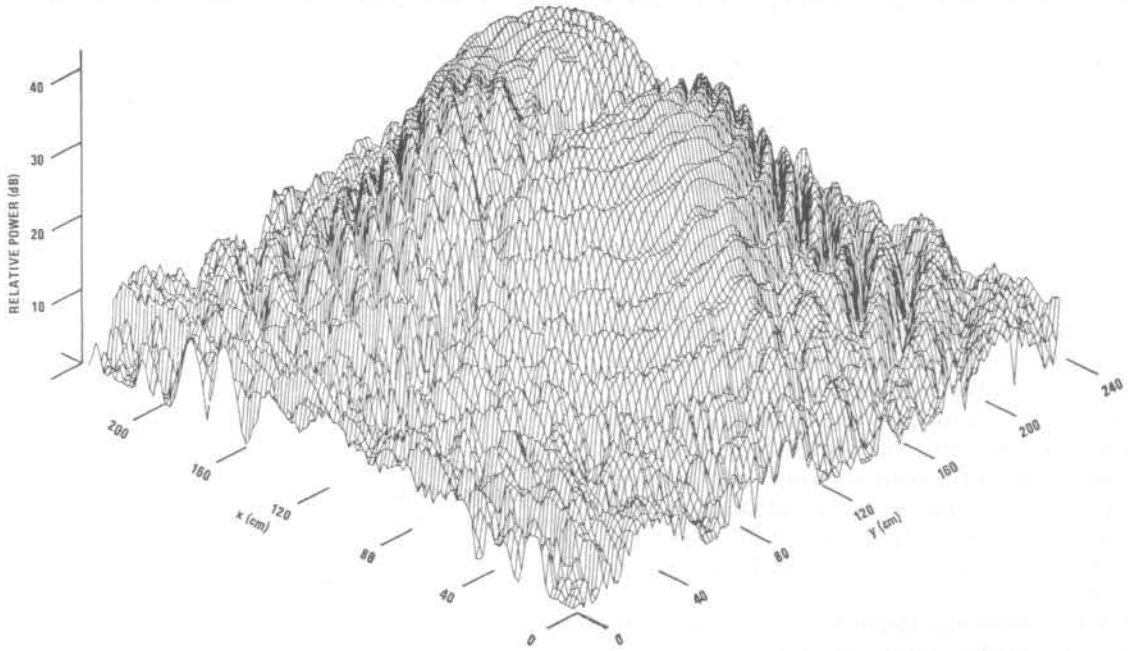

Fig. 8. Near-field amplitude distribution for azimuth (only) monopulse antenna. Difference pattern at 5.45 GHz.

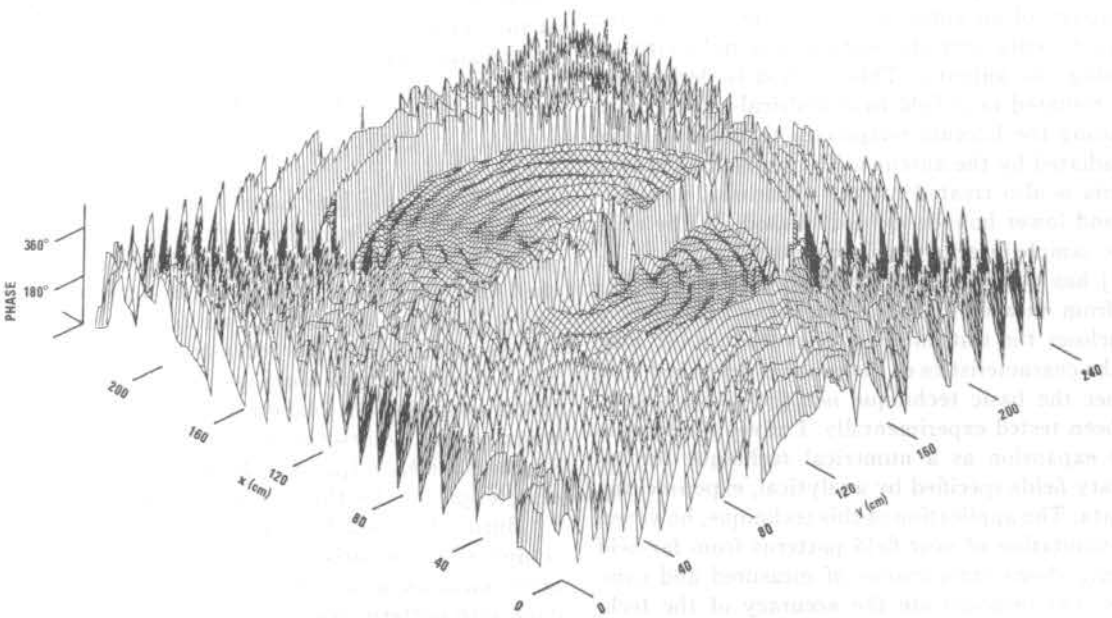

Fig. 9. Near-field phase distribution for azimuth (only) monopulse antenna. Difference pattern at 5.45 GHz.

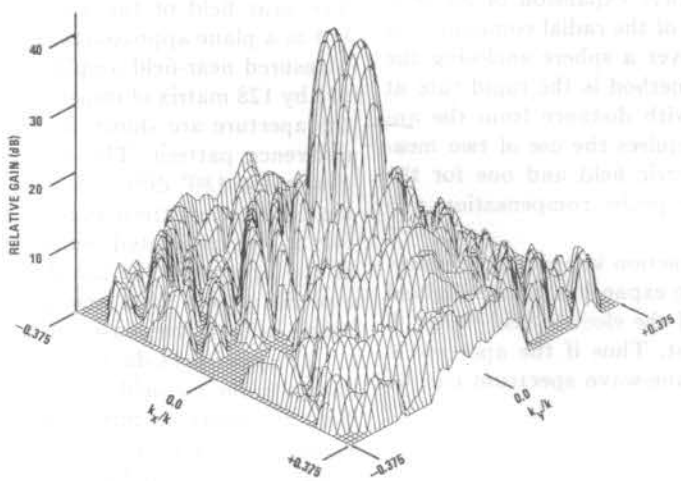

Fig. 10. Computed far-field difference pattern in wavenumber space for azimuth (only) monopulse antenna operating at 5.45 GHz. Along each principal plane ($k_x = 0$ or $k_y = 0$), the angular section is approximately $\pm 22°$.

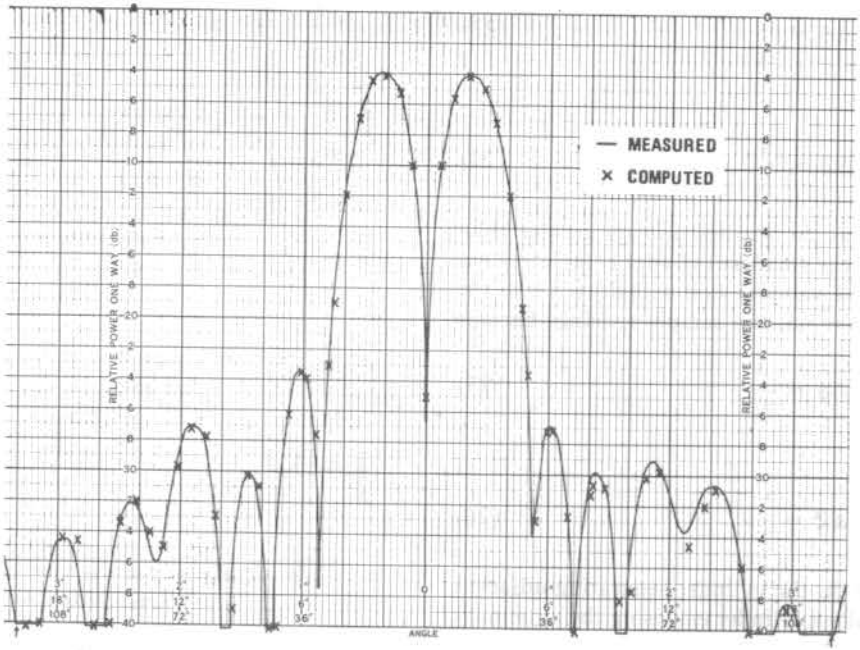

Fig. 11. Comparison of measured far-field pattern and computed far-field pattern over a ±20° secto in principal azimuth plane of monopulse difference pattern at 5.45 GHz.

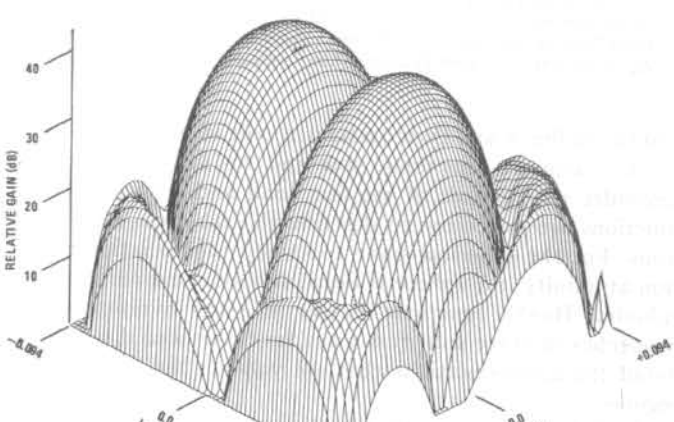

Fig. 12. High-resolution plot of main beam region of pattern in wavenumber space for azimuth (only) monopulse antenna operating at 5.45 GHz. Along each principal plane ($k_x=0$ or $k_y=0$), the angular sector is approximately ±5°

standard gain horn, and an electrically tenna. It is their opinion that because of t cal structure and the experimental docu calculated far-field results obtained by a expansion method to near-field measurem accurate and as easily obtained as any re pleteness that could be obtained from d surements.

Cylindrical-Wave Expansion: It can cylindrical-wave spectrum of an antenn from the output of a probe used to mea electric field on the surface of a right ci closing the antenna. The cylindrical-wav probe can be used to modify the measur test antenna to compensate for the noni of the probe. When the method of steepes to approximate the far field of the cylindri Leach [41] shows the result is

$$E_R = 0$$

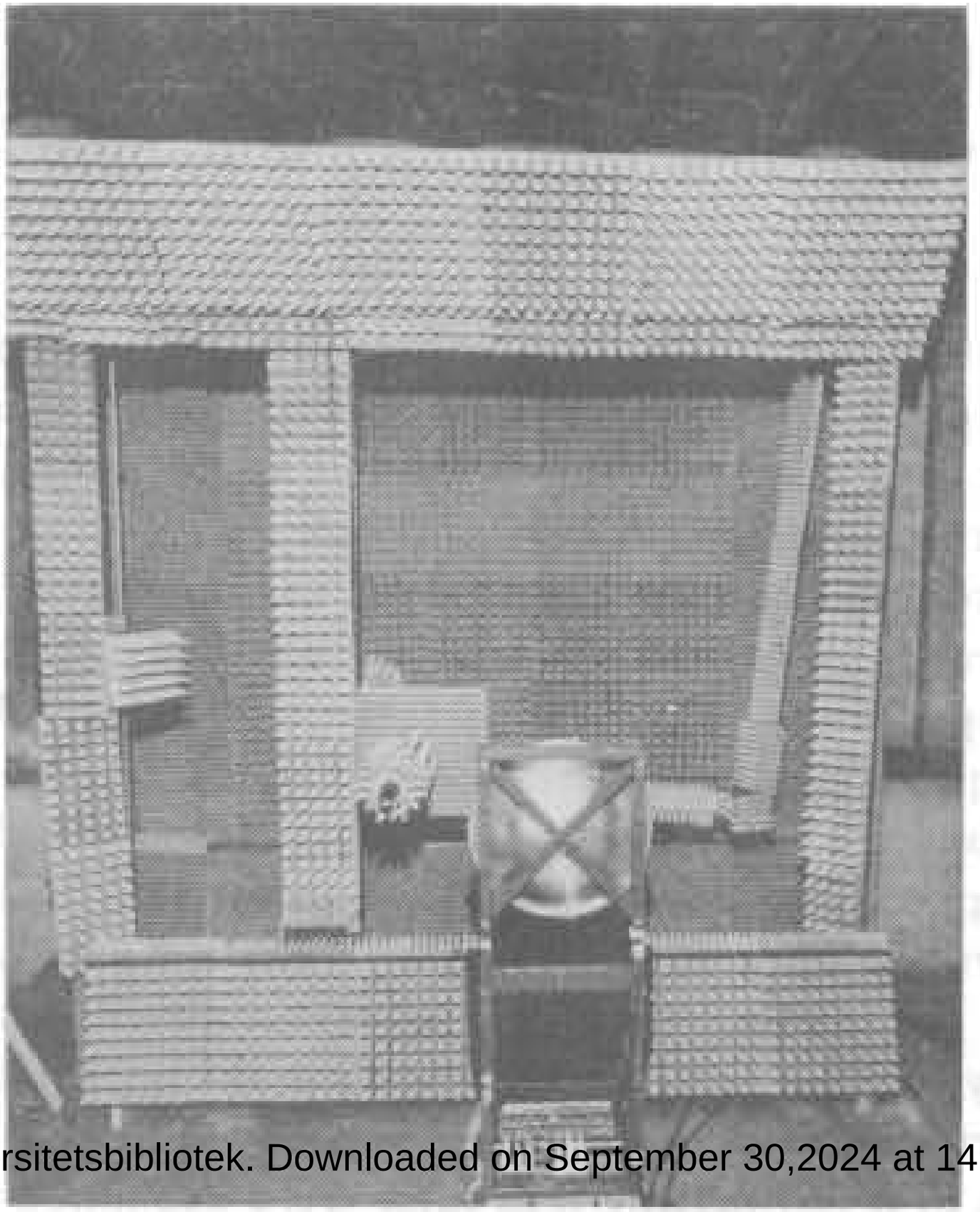

Fig. 15. Front view of near-field probe and x–y–z positioner.

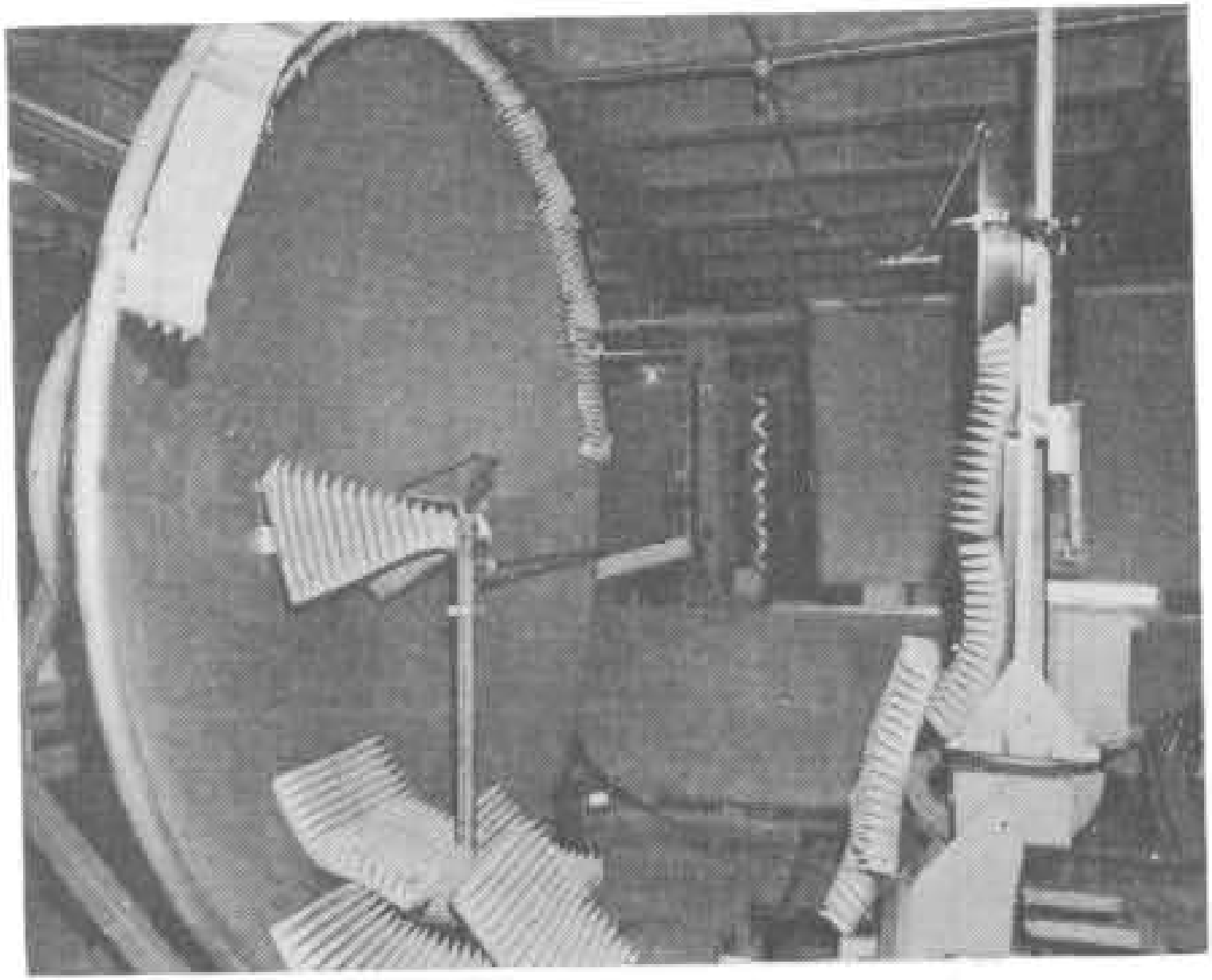

Fig. 17. Photograph of a point-source compact range with a paraboloidal reflector test antenna in position.

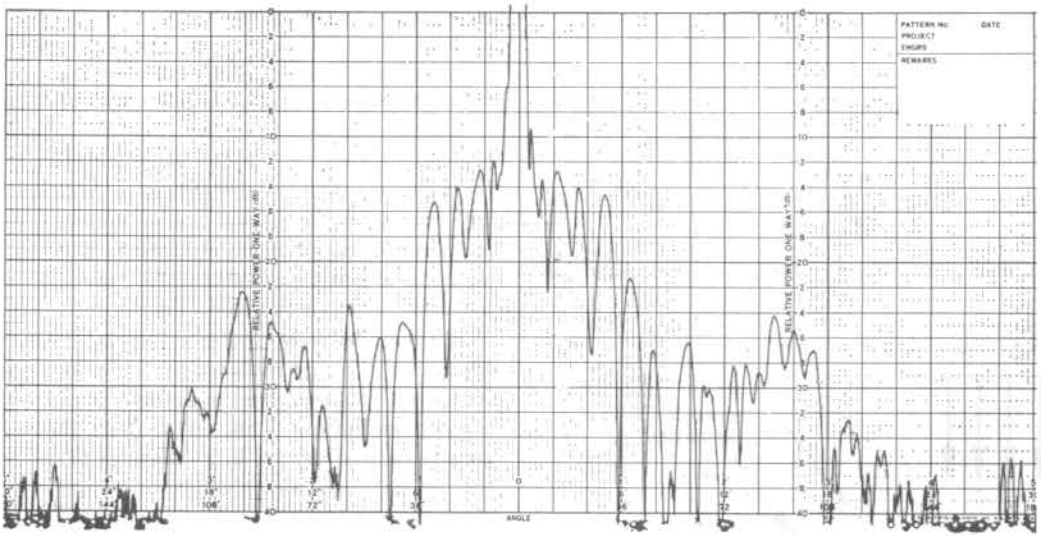

(a)

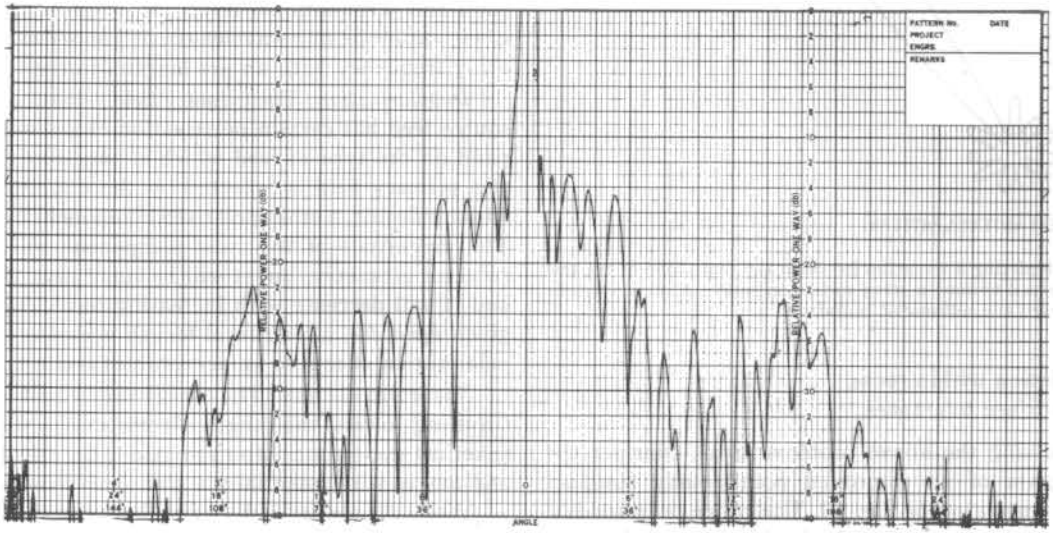

(b)

Fig. 19. Azimuth patterns (H plane) measured on a far-field outdoor range and on a point-source compact range. The antenna was a 76-cm paraboloidal reflector with a horn feed operating at 10 GHz. The gain level at the top of each chart is -15 dB relative to the peak of the main lobe. (a) Outdoor range. (b) Compact range.

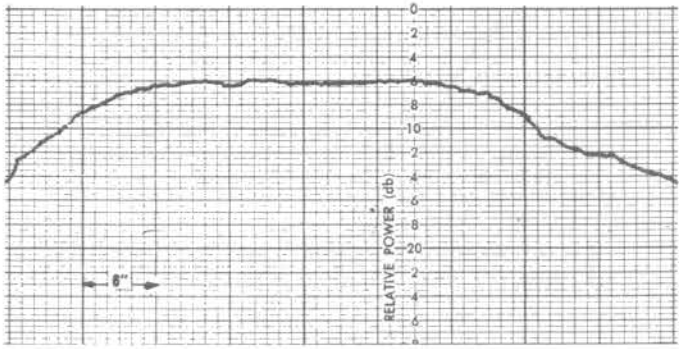

Fig. 22. Power density distribution with vertical polarization at 10 GHz for a vertical cut in the test volume of a line-source compact range.

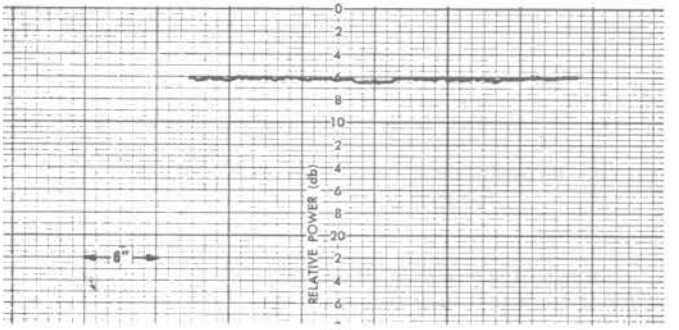

(a)

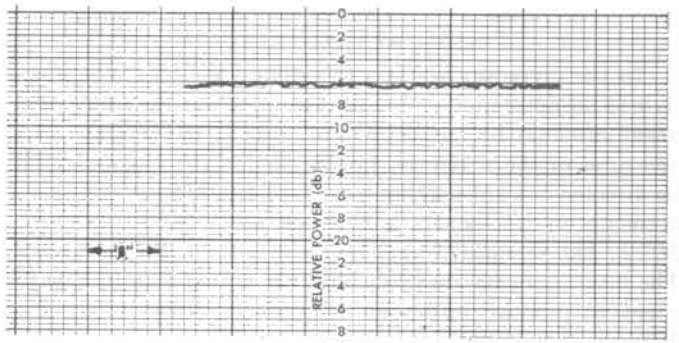

(b)

the test volume of a line-source compact range. Vertical polarization at 10 GHz. (a) Center of range-reflector aperture. (b) 25.4 cm above center of range-reflector aperture.

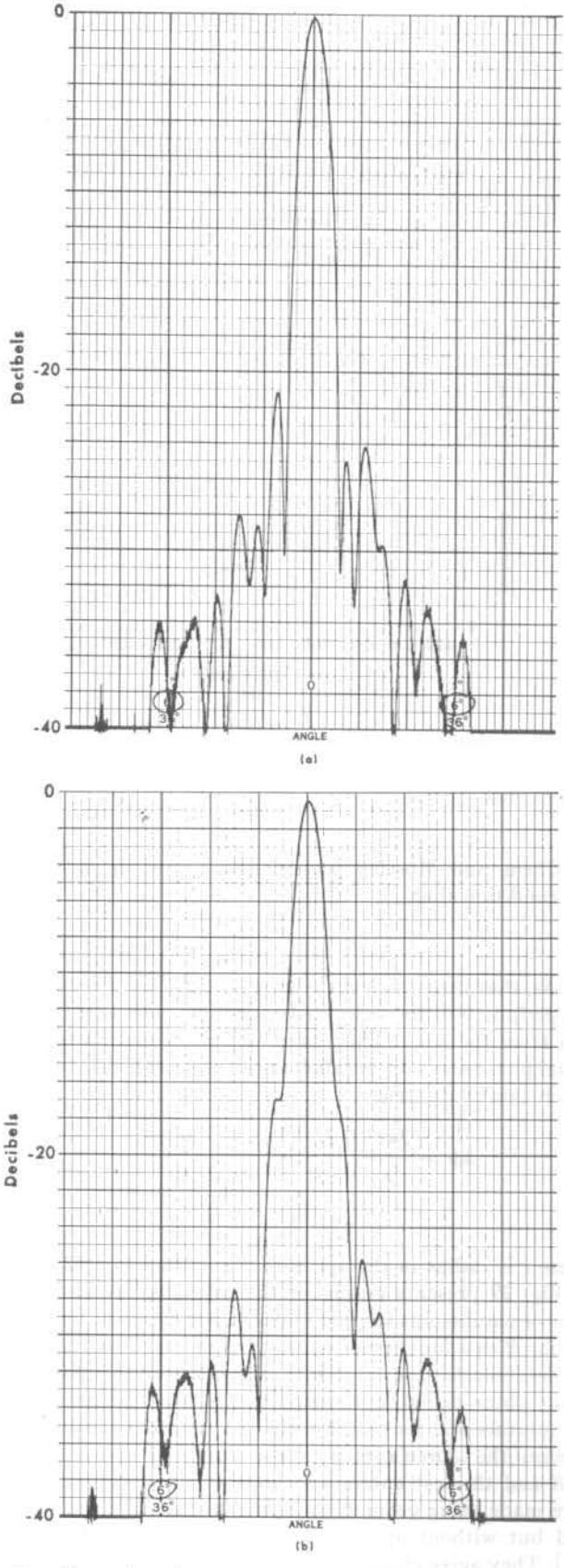

Fig. 26. Illustration of pattern distortion for typical paraboloid. (a) Focused at $5D^2/6\lambda$ and measured at the same range. (b) Focused at infinity and measured again at $5D^2/6\lambda$ to simulate operation at infinity after focusing at the shorter range.

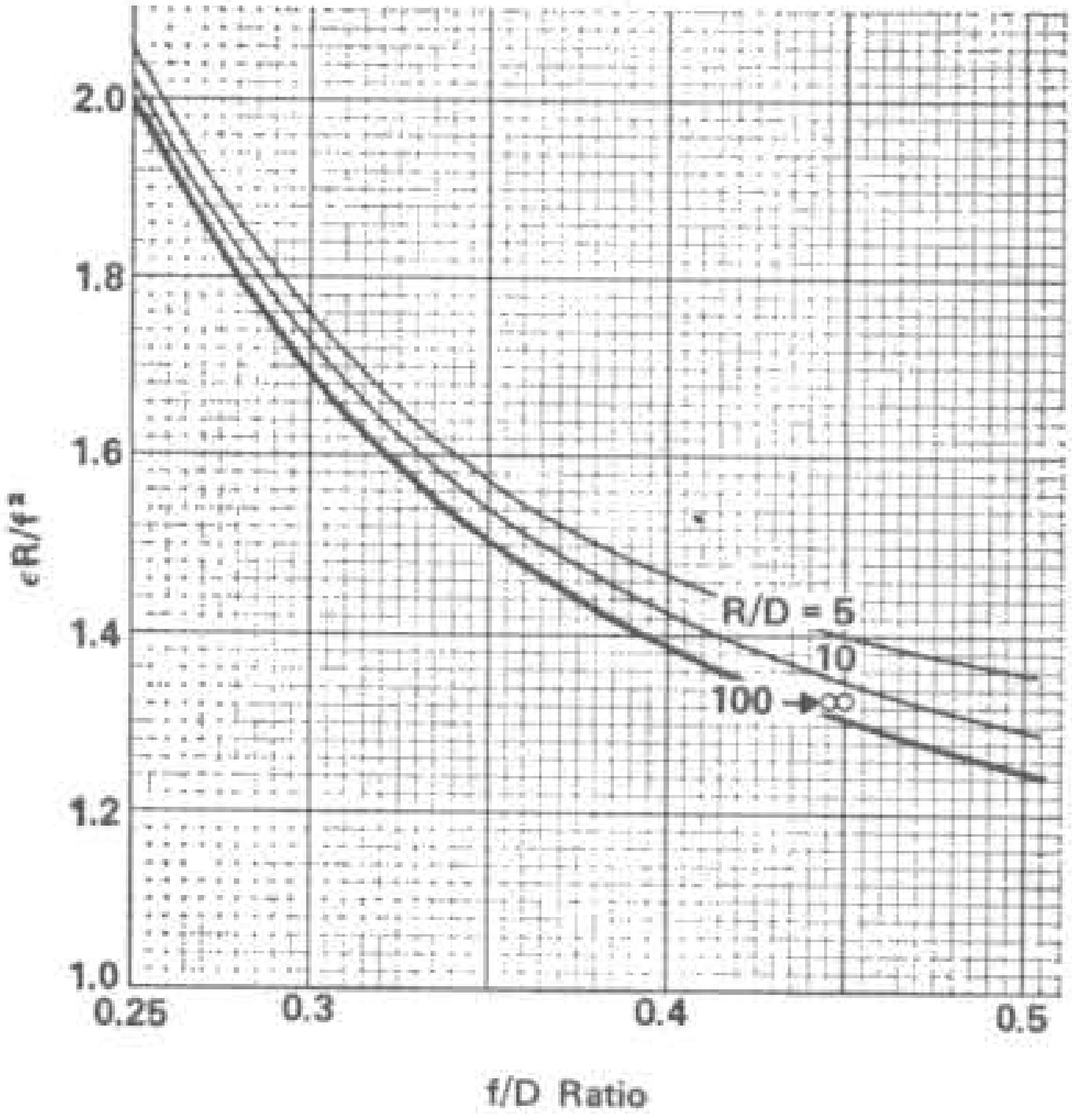

Fig. 30. Axial feed movement ϵ required to refocus paraboloid of focal length f and diameter D to infinity after focusing at test separation R. Curves are based on geometrical optics approach.